



Trends in peroxyacetyl nitrate (PAN) in the upper troposphere and lower stratosphere over southern Asia during the summer monsoon season: regional impacts

S. Fadnavis¹, M. G. Schultz², K. Semeniuk³, A. S. Mahajan¹, L. Pozzoli⁴, S. Sonbawne¹, S. D. Ghude¹, M. Kiefer⁵, and E. Eckert⁵

¹Indian Institute of Tropical Meteorology, Pune, India

²Institute of Energy and Climate Research – Troposphere (IEK-8), Forschungszentrum Jülich, Jülich, Germany

³Department of Earth and Space Sciences and Engineering, York University, Toronto, Canada

⁴Eurasia Institute of Earth Sciences, Istanbul Technical University, Istanbul, Turkey

⁵Karlsruhe Institute of Technology, Institute for Meteorology and Climate Research, Karlsruhe, Germany

Correspondence to: S. Fadnavis (suvarna@tropmet.res.in)

Received: 18 June 2014 – Published in Atmos. Chem. Phys. Discuss.: 22 July 2014

Revised: 9 October 2014 – Accepted: 28 October 2014 – Published: 4 December 2014

Abstract. We analyze temporal trends of peroxyacetyl nitrate (PAN) retrievals from the Michelson Interferometer for Passive Atmospheric Sounding (MIPAS) during 2002–2011 in the altitude range 8–23 km over the Asian summer monsoon (ASM) region. The greatest enhancements of PAN mixing ratios in the upper troposphere and lower stratosphere (UTLS) are seen during the summer monsoon season from June to September. During the monsoon season, the mole fractions of PAN show statistically significant (at 2σ) positive trends from 0.2 ± 0.05 to 4.6 ± 3.1 ppt yr⁻¹ (except between 12 and 14 km) which is higher than the annual mean trends of 0.1 ± 0.05 to 2.7 ± 0.8 ppt yr⁻¹. These rising concentrations point to increasing NO_x (= NO + NO₂) and volatile organic compound (VOC) emissions from developing nations in Asia, notably India and China.

We analyze the influence of monsoon convection on the distribution of PAN in UTLS with simulations using the global chemistry–climate model ECHAM5-HAMMOZ. During the monsoon, transport into the UTLS over the Asian region primarily occurs from two convective zones, one the South China Sea and the other over the southern flank of the Himalayas.

India and China host NO_x-limited regimes for ozone photochemical production, and thus we use the model to evaluate the contributions from enhanced NO_x emissions to the changes in PAN, HNO₃ and O₃ concentrations in the

UTLS. From a set of sensitivity experiments with emission changes in particular regions, it can be concluded that Chinese emissions have a greater impact on the concentrations of these species than Indian emissions. According to SCanning Imaging Absorption SpectroMeter for Atmospheric CHarotography (SCIAMACHY) NO₂ retrievals NO_x emissions increases over India have been about half of those over China between 2002 and 2011.

1 Introduction

The boreal summer monsoon circulation over the polluted land mass of Asia vents chemical constituents from the boundary layer into the upper troposphere and lower stratosphere (UTLS), where they are re-distributed over a wide region in the subtropical latitudes (Gottelman et al., 2004; Park et al., 2004, 2007; Li et al., 2005; Randel and Park, 2006; Fu et al., 2006; Xiong et al., 2009; Randel et al., 2010; Fadnavis et al., 2013). The chemical constituents in the UTLS influence the radiative balance and heat transport in the atmosphere (Ravishankara, 2012; Fadnavis et al., 2013). For example, monsoon injection contributes ~75 % of the total net upward water vapor flux in the tropics at tropopause levels (Gottelman et al., 2004). The increased amount of water vapor in the lower stratosphere could enhance ozone deple-

tion and thus raise ultraviolet radiation levels at Earth's surface (Anderson et al., 2012). Satellite observations show convective transport and mixing of chemical constituents (e.g., aerosols, CO, NO_x, CH₄ and HCN) in the tropical tropopause region during the Asian summer monsoon (ASM) season (Dodion et al., 2008; Park et al., 2009; Randel et al., 2010; Vernier et al., 2011). In the stratosphere, these chemical constituents are transported to the southern subtropics by the Brewer–Dobson circulation (Park et al., 2004; Fadnavis et al., 2013) and they affect ozone, water vapor and aerosol-related constituents in the global stratosphere (Randel et al., 2010; Randel and Jensen, 2013). Peroxyacetyl nitrate (PAN) is one such chemical species important in the tropical UTLS over the south Asian regions for two reasons: (1) it is a secondary pollutant with implications for the production of tropospheric ozone (O₃); (2) PAN is also a useful tracer for diagnosing transport due to monsoon convection and understand the redistribution of NO_x in the global stratosphere.

PAN mixing ratios vary from less than 1 pptv in the remote marine atmosphere (as observed in NASA GTE PEM-Tropics B campaign in the South Pacific lower marine boundary layer, data available at <http://acd.ucar.edu/~emmons/DATACOMP/>) to several ppbv in the polluted urban environment and biomass burning plumes (Ridley et al., 1992; Singh et al., 1998). In the UTLS, mixing ratios are typically in the range 10–300 pptv (Emmons et al., 2000; Keim et al., 2008). PAN is formed exclusively from the chemical reaction of peroxyacetyl radicals (CH₃C(O)OO) with NO₂. The peroxyacetyl radical is generated from the oxidation of acetaldehyde (CH₃CHO) by OH, or through photolytic decomposition of acetone (CH₃COCH₃) and methylglyoxal (CH₃COCHO), which are secondary pollutants, produced by oxidation of other non-methane volatile organic compounds (NMVOCs) such as propene (C₃H₆). In the upper troposphere, photolysis of acetone (CH₃COCH₃) is an important source of peroxyacetyl radicals (Fischer et al., 2013). The main loss reactions of PAN are thermal decomposition (most important in the lower troposphere up to ~500 hPa), photolysis (most important in the UTLS and above) and the reaction with OH. All of these reactions lead to the formation of reactive nitrogen compounds: the first two reactions yield NO₂, while the reaction with OH yields NO₃ as a product. At the surface, PAN can also be deposited. Its dry deposition velocity is on the order of 0.5 cm s⁻¹ during daytime and 0.1 cm s⁻¹ during nighttime (Wu et al., 2012).

Rapid industrialization, traffic growth and urbanization in Asia cause increasing emissions of ozone precursors including NO_x and VOCs. These emissions are projected to increase through 2020 in spite of the efforts of Asian countries to combat air pollution problems (Ohara et al., 2007). Most parts of Asia are NO_x limited regions, i.e., controlling NO_x in these regions would reduce ozone concentrations (Yamaji et al., 2006; Sinha et al., 2014). India and China are by far the largest emitters in Asia. Satellite observations by the SCanning Imaging Absorption SpectroMeter for Atmo-

spheric CHartography (SCIAMACHY) and Ozone Monitoring Instrument (OMI) exhibit positive trends of ~3.8 % yr⁻¹ in tropospheric column NO₂ over India (Ghude et al., 2013) and 7.3 (± 3.1) % yr⁻¹ over China (Schneider and van der A, 2012). Although there is debate if these observed NO_x changes could be directly related to emission changes, there is no doubt that increased NO_x concentrations can enhance the formation of PAN, some of which is then transported into the UTLS by the Asian summer monsoon (ASM) circulation. In addition to PAN being transported from the polluted boundary layer, it can also be formed in the upper troposphere through the production of NO_x from lightning (Tie et al., 2001; Zhao et al., 2009). Lightning activity over southern Asia is highest during the monsoon season (Ranalkar and Chaudhari, 2009; Penki and Kamra 2013). The estimated global NO_x production by lightning is ~3 Tg N yr⁻¹ (Nesbitt et al., 2000; Tie et al., 2002). Simulations with the model of ozone and related tracers (MOZART) show an increase in UTLS PAN over the ASM region due to lightning by 20–30 % (Tie et al., 2001).

Thus it is interesting to examine the influence of Asian monsoon convection on the distribution of PAN in the global UTLS. Also, the impact of enhanced NO_x emissions from India and China on the redistribution of PAN and other related chemical species in the global UTLS merits attention. Due to the NO_x limitation in India and China, the impact of enhanced VOC emissions on the distribution of PAN is expected to be smaller. Investigating this in more detail goes beyond the scope of this study because one would have to define a credible VOC speciation and its changes over time. We employ the state-of-the-art ECHAM5-HAMMOZ (European Centre General Circulation Model version5, ECHAM5, aerosols Hamburg Module, HAM, and chemistry from MOZART-2, MOZ) chemistry climate model (Roeckner et al., 2003; Horowitz et al., 2003; Stier et al., 2005) and perform sensitivity simulations in order to investigate the relative contributions from India and China to the increased UTLS PAN concentrations. The paper is organized as follows: data analysis, model description and setup are described in Sect. 2. In Sect. 3, we discuss the distribution of PAN in the UTLS during the ASM from satellite measurements and its transport from model simulations. Section 4 contains satellite-observed trends in PAN over India and China. The impact of enhanced anthropogenic Asian NO_x on PAN, HNO₃ and ozone are discussed in Sect. 5. Conclusions are given in Sect. 6.

2 Data and analysis

2.1 Satellite measurement

The MIPAS-E instrument onboard the ENVironmental SATellite (ENVISAT) was launched in March 2002 into a polar orbit of 800 km altitude, with an orbital period of

about 100 min and an orbit repeat cycle of 35 days. MIPAS-E (Fischer and Oelhaf, 1996; Fischer et al., 2008) was a Fourier transform spectrometer that provided continual limb emission measurements in the mid-infrared over the range 685–2410 cm^{-1} (14.6–4.15 μm). From June 2002 to March 2004, MIPAS operated in its full spectral resolution mode at an un-apodized resolution of 0.035 cm^{-1} , and with tangent altitude steps of 3 km in the UTLS. From January 2005 through the end of the mission the spectral resolution was reduced to 0.0875 cm^{-1} , while the tangent altitude steps in the UTLS were reduced to 1.5–2 km. Until the platform's failure in April 2012, MIPAS monitored atmospheric minor constituents affecting atmospheric chemistry including PAN, NO_x and O_3 . The details of the general retrieval method and setup, error estimates and use of averaging kernel and visibility flag are documented by Von Clarmann et al. (2009). Details of the PAN retrievals, error budget and vertical resolution are given by Glatthor et al. (2007) for the 2002–2004 measurement period for data version V3O_PAN_5, and by Wiegele et al. (2012) for the 2005–2012 measurement period for data version V5R_PAN_220/V5R_PAN_221 (different 220/221 naming due to technical reasons). The total error of PAN retrievals is below 20 % from 10–12 km, below 30 % from 12–16 km and below 40 % above 16 km for V3O_PAN_5 (see Fig. 2 in Glatthor et al., 2007). The error is dominated by contributions of spectral noise and the uncertainty of the instrument pointing. Table 3 in Wiegele et al. (2012) indicates that for the V5R_PAN_220/221 product, the total error is below 10 % from 10–12 km and above 100 % for altitudes greater than 15 km. Again, spectral noise and the uncertainty of the instrument pointing are the main contributors.

The sensitivity of the PAN retrievals can be judged by the averaging kernels. Since two types of retrievals are used in this study, V3O_PAN_5 and V5R_PAN_220/221 from high and reduced spectral resolution, respectively, we give two examples of the respective averaging kernel rows. The locations of the examples are 26° N and 81° E for the V3O_PAN_5 example and 28° N and 85° E for V5R_PAN_220. Figure S1a and b in the Supplement shows the rows of the averaging kernels for an altitude range of 5 to 25 km. The diamonds indicate the respective nominal altitudes of the retrieval grid. Figure S1 in the Supplement shows that the retrieval results below 8–9 km are dominated by information from above the nominal altitude. A similar, albeit less obvious, situation develops for altitudes above 22–23 km. There and above the information has an increasing weight from lower than nominal altitudes. This is the reason why the MIPAS PAN data is not considered below 8 km and above 23 km. Another effect clearly visible in both example plots is that the altitude region which influences the retrieved PAN value at a given altitude is increasing with altitude, i.e., the vertical resolution decreases with altitude. To account for the comparatively low and altitude-dependent vertical resolution, the model data

to be directly compared to MIPAS measurements was convolved with the MIPAS PAN averaging kernel.

In this study we analyze the MIPAS-E-observed PAN data during the period 2002–2011. The data can be accessed at http://share.lsd.fkit.edu/imk/asf/sat/mipas-export/Data_by_Target/. The data versions used are V3O_PAN_5 for 2002–2004, and V5R_PAN_220/V5R_PAN_221 for 2005–2011. The data is processed as per the quality specifications given in the documentation. The useful height range is specified as 5 to 23 km. The data are contoured and gridded at 8° longitude and 4° latitude resolution.

2.2 ECHAM5-HAMMOZ model simulation and experimental setup

The ECHAM5-HAMMOZ aerosol–chemistry–climate model used in the present study comprises of the general circulation model ECHAM5 (Roeckner et al., 2003), the tropospheric chemistry module, MOZ (Horowitz et al., 2003) and the aerosol module, Hamburg Aerosol Model (HAM) (Stier et al., 2005). The gas phase chemistry is based on MOZART-2 model (Horowitz et al., 2003) chemical scheme, which includes a detailed chemistry of O_x – NO_x hydrocarbons with 63 tracers and 168 reactions. The radiative transfer calculation considers the simulated concentrations of both ozone and aerosols. The $\text{O}(^1\text{D})$ quenching reaction rates were updated according to Sander et al. (2003), and the isoprene nitrates chemistry according to Fiore et al. (2005). In the MOZART chemical mechanism, the PAN formation process occurs through the reaction of peroxyacetyl radical (CH_3CO_3) and NO_2 . This reaction is reversible, and the thermal decomposition of PAN back to CH_3CO_3 and NO_2 is the main sink of PAN. The reaction rates for this reversible reaction are updated according to Sander et al. (2006). CH_3CO_3 is mainly formed by oxidation of acetaldehyde (CH_3CHO) by OH, and by the photolytic decomposition of acetone (CH_3COCH_3) and methylglyoxal (CH_3COCHO). In the model simulations, we included emissions of acetone from anthropogenic sources and wild fires (primary sources), while acetaldehyde and methylglyoxal are produced by the oxidation of other NMVOCs (secondary sources). In particular, oxidation of primary NMVOCs like ethane (C_2H_6), propane (C_3H_8) and propene (C_3H_6) forms acetaldehyde, while CH_3COCHO is mainly formed from the oxidation products of isoprene and terpenes. Higher acyl peroxy nitrates (MPAN) are included in MOZART-2 chemical scheme, they are also formed through oxidation of NMVOCs, but their production is not significant compared to PAN. The main loss process of PAN from the atmosphere is the thermal decomposition into its precursors. Other loss processes are photolysis and reaction with OH. In ECHAM5-HAMMOZ, dry deposition follows the scheme of Ganzeveld and Lelieveld (1995). Soluble trace gases such as HNO_3 and SO_2 are also subject to wet deposition. In-cloud and below-cloud scavenging follows the scheme described

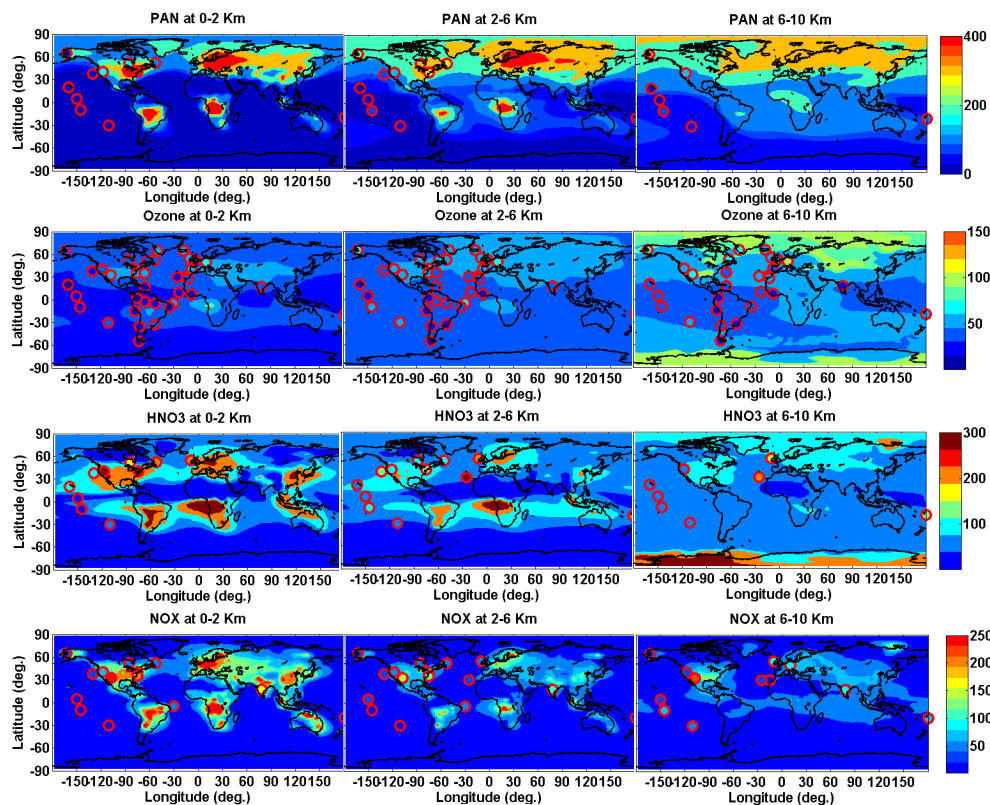


Figure 1. Global mean distribution of PAN (ppt), ozone (ppb), HNO₃ (ppt) and NO_x (ppt) averaged for the monsoon season and altitude ranges. Model results from reference simulation (background solid contours) are compared with aircraft observations from Table 1 for all the years (filled circles). Aircraft observations are averaged vertically and horizontally over the coherent regions.

by Stier et al. (2005). PAN is not highly water soluble, therefore wet deposition is a minor removal process, and dry deposition is also not significant.

The model is run at a spectral resolution of T42 corresponding to about $2.8^\circ \times 2.8^\circ$ in the horizontal dimension and 31 vertical hybrid σ - p levels from the surface up to 10 hPa. The details of model parameterizations, emissions and validation are described by Fadnavis et al. (2013), Pozzoli et al. (2008a, b, 2011). Here, we note that our base year for aerosol and trace gas emissions is 2000. Each member of our sensitivity study consists of continuous simulations for 10 years from 1995 to 2004. Emissions were the same in each simulation, and meteorology varied because of different sea surface temperature (SST) and sea ice (SIC) data. The AMIP2 SSTs and SIC representative of the period 1995–2004 were specified as a lower boundary condition.

In order to understand the impact of enhanced anthropogenic NO_x emissions on the distributions of PAN, HNO₃ and ozone in the UTLS, we conducted six simulations for the period 1995–2004: (1) a reference experiment and five sensitivity experiments (referred to as experiments 2–6), where NO_x emissions over India and China were scaled according to the observed trends. Experiment (2) increases NO_x emissions over India by 38 % (Ind38), run (3) increases those

over China by 73 % (Chin73). Experiment (4) shows the effect of the combined changes (India by 38 %, China by 73 %) (Ind38Chin73). Experiment (5) assumes equal relative changes of NO_x emissions (India by 38 %, China by 38 %) (Ind38Chin38) in order to analyze the respective contributions, and to understand the regional emission enhancement impact on the UTLS for same emission enhancement over China. In experiment (6), emissions are increased over India by 73 % (Ind73) to analyze the impact of Indian emissions with equal emissions from China. The emission perturbations were derived from observed NO₂ trends of ~ 3.8 % per year over India (Ghude et al., 2013) and $7.3 (\pm 3.1)$ % per year over China (Schneider and van der A, 2012). Similar values of NO₂ trends (5 – 10 % yr⁻¹) are also reported by Hilboll et al. (2013) over megacities of India and China.

3 Results and discussions

3.1 Comparison with aircraft and ozonesonde measurements

Model-simulated PAN, NO_x, HNO₃ and Ozone mixing ratios are evaluated with climatological datasets of airborne campaigns during the monsoon season (June–September).

Table 1. Global aircraft measurements used for model evaluation.

Experiment	Date frame	Species	Location
POLINAT-2 (Falcon)	Sep 19–Oct 25, 1997	O ₃ , NO _x	Canary Islands: lat = 25, 35 long = 340, 350 Eastern Atlantic: lat = 35, 45 long = 330, 340 Europe: lat = 45, 55 long = 5, 15 Ireland: lat = 50, 60 long = 345, 355
PEM-Tropics-A (DC8)	Aug 24–Oct 15, 1996	O ₃ , NO _x , HNO ₃ , PAN	Christmas Island: lat = 0, 10 long = 200, 220 Easter Island: lat = -40, -20 long = 240, 260 Fiji: lat = -30, -10 long = 170, 190 Hawaii: lat = 10, 30 long = 190, 210 Tahiti: lat = -20, 0 long = 200, 230
PEM-Tropics-A (P3)	Aug 15–Sep 26, 1996	O ₃ , HNO ₃	Christmas Island: lat = 0, 10 long = 200, 220 Easter Island: lat = -40, -20 long = 240, 260 Hawaii: lat = 10, 30 long = 190, 210 Tahiti: lat = -20, 0 long = 200, 230
ABLE-3B (Electra)	Jul 6–15, 1990	O ₃ , NO _x , HNO ₃ , PAN	Labrador: lat = 50, 55 long = 300, 315 Ontario: lat = 45, 60 long = 270, 280 US East Coast: lat = 35, 45 long = 280, 290
CITE-3 (Electra)	Aug 22–Sep 29, 1989	O ₃ , NO _x	Natal: lat = -15, 5 long = 325, 335 Wallops: lat = 30, 40 long = 280, 290
ELCHEM (Sabreliner)	Jul 27–Aug 22, 1989	O ₃ , NO _x	New Mexico: lat = 30, 35 long = 250, 255
ABLE-3A (Electra)	Jul 7–Aug 17, 1988	O ₃ , NO _x , PAN	Alaska: lat = 55, 75 long = 190, 205
ABLE-2A (Electra)	Jul 12–Aug 13, 1985	O ₃	Eastern Brazil: lat = -10, 0 long = 300, 315 Western Brazil: lat = -5, 0 long = 290, 300
STRATOZ-3 (Caravelle 116)	Jun 4–26, 1984	O ₃	Brazil: lat = -20, 0 long = 315, 335 Canary Islands: lat = 20, 35 long = 340, 355 E Tropical N Atlantic: lat = 0, 20 long = 330, 345 England: lat = 45, 60 long = -10, 5 Goose Bay: lat = 45, 60 long = 290, 305 Greenland: lat = 60, 70 long = 290, 330 Iceland: lat = 60, 70 long = 330, 355 NW South America: lat = -5, 10 long = 275, 295 Puerto Rico: lat = 10, 25 long = 290, 300 S South America: lat = -65, -45 long = 275, 300 SE South America: lat = -45, -20 long = 295, 320 SW South America: lat = -45, -25 long = 285, 292. Spain: lat = 35, 45 long = -15, 0 West Africa: lat = 0, 15 long = -15, 0 W South America: lat = -25, -5 long = 275, 290 Western N Atlantic: lat = 25, 45 long = 290,300
CITE-2 (Electra)	Aug 11–Sep 5, 1986	O ₃ , NO _x , HNO ₃ , PAN	California lat = 35, 45 long = 235, 250 Pacific: lat = 30, 45 long = 225, 235
CAIPEEX	Sep 2009 and Oct 2010	O ₃ , NO _x	lat = 17° N, long = 78° E

The data were retrieved from <http://acd.ucar.edu/~emmons/DATACOMP/CAMPAIGNS/>. The NO_x and ozone volume mixing ratios observed during Cloud Aerosol Interaction & Precipitation Enhancement Experiment (CAIPEEX) experiment, September 2010, are evaluated over the Indian region. The details of instrument and measurement techniques are available at <http://www.tropmet.res.in/~caipeex/about-data.php>. The list of data sets and aircraft campaigns are presented in Table 1. For comparison, aircraft observations are averaged over 0–2 km, 2–6 km and 6–8 km and at the coherent latitude and longitude of the flight region. Model simulations are also averaged at the same altitudes. Figure 1a–k com-

pare the observed global distribution of PAN, ozone, HNO₃ and NO_x to those simulated by ECHAM5-HAMMOZ. The mean aircraft observations are shown as filled circles and model output are background contours. Figure 1 indicates that model-simulated PAN, HNO₃ and NO_x show good agreement with aircraft measurements. Figure S2 in the Supplement indicates the model bias (ECHAM5-HAMMOZ aircraft observations) in PAN, ozone, HNO₃ and ozone. The model bias is different at each location. It varies with species and altitude. Between 0 and 2 km, simulated PAN shows positive bias ~7–12 ppt in the western Pacific, 52–105 ppt over the United States of America (USA). Ozone shows positive

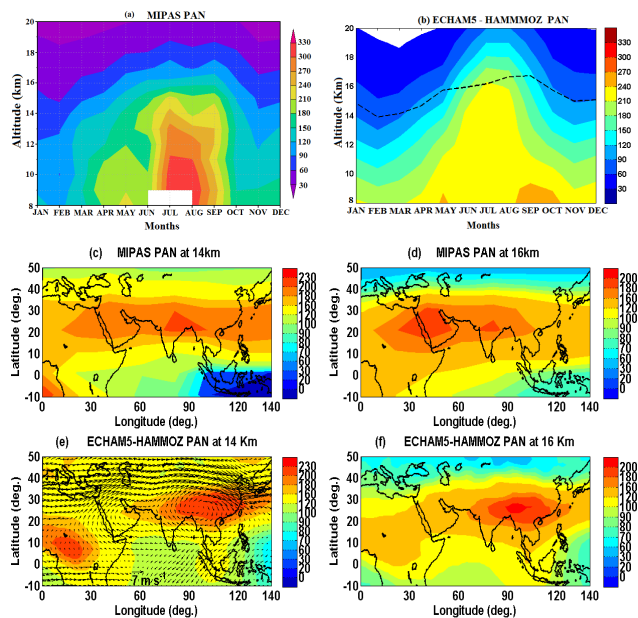


Figure 2. The monthly distribution of PAN (ppt) averaged over the anticyclone region (60–120° E, 10–40° N) (a) as observed by MIPAS and for the period 2002–2011 (b) ECHAM5-HAMMOZ reference simulation. Distribution of seasonal mean PAN concentration (ppt) as observed by MIPAS (climatology for the period 2002–2011) at (c) 14 km (d) 16 km and ECHAM5-HAMMOZ reference simulation at (e) 14 km (f) 16 km. ECHAM5-HAMMOZ simulation is smoothed with averaging kernel of MIPAS.

bias ~ 7 ppb over India, ~ 3 –15 ppb over the western Pacific, negative bias ~ 2 –20 ppb in mid-latitude Atlantic and positive bias 2–20 ppb over tropical Atlantic, ~ 2 –18 ppb over the USA. HNO_3 is higher by ~ 20 –75 ppt over the western Pacific and lower by ~ 5 ppt at few locations. Over the USA bias is negative less than 5 ppt. NO_x shows positive bias ~ 40 ppt over India and 0–10 ppt over the western Pacific. Between 2–6 m and 6–10 km, over the western Pacific simulated PAN show negative bias ~ 10 –20 ppt and positive bias ~ 5 –50 ppt at some locations. Over the USA bias values are ~ 4 –70 ppt. Ozone is lower by ~ 10 –15 ppb and higher by ~ 3 –30 ppb at some locations in the western Pacific, 3–30 ppb over Atlantic and ~ 2 –30 ppb over the USA. The positive bias in HNO_3 reduces to 3–20 ppt and negative bias to 3 to 20 ppt over the western Pacific, over the USA negative bias is ~ 20 ppt and positive bias is ~ 3 –70 ppt. The NO_x shows negative bias ~ 40 ppt over India. The bias values vary between 6 and 10 ppt over the western Pacific, 15 and -20 ppt over the USA and Atlantic. As can be seen from above discussions, ozone exhibits a low bias over South America and the Atlantic (for 0–6 km). Model-simulated ozone and NO_x show good agreement with CAIPEEX measurements over the Indian region. Model-simulated seasonal mean ozone is compared with ozonesonde measurements (2000–2009) over three distributed stations, where verti-

cal profiles are available for long periods (1) near equator (Thiruvananthapuram: 8.4875° N, 76.9525° E), (2) tropical (Pune: 18.52° N, 73.85° E) and (3) subtropical stations (Delhi: 28.61° N, 77.23° E) over India. The simulated ozone profiles are extracted at the grid square nearest the center of the above three stations. Figure S3 in the Supplement depicts that simulated ozone show fairly good agreement with ozonesonde measurements over all the three stations: in general, simulated ozone is less than that of ozonesonde measurements except at Delhi (between 200 and 100 hPa). At Delhi, simulated ozone is less than that of ozonesonde by ~ 3 –40 ppb in the troposphere and by 1000–4000 ppb in the lower stratosphere. The differences are larger at Pune (troposphere ~ 20 –120 ppb, stratosphere ~ 900 –2500 ppb) and lesser at Thiruvananthapuram (troposphere ~ 10 –30 ppb and stratosphere 300–1300 ppb). This may be due to differences in spatial coverage. The ozonesonde measurements are at the stations (although ozonesonde drifts horizontally) while model simulations are made at the grid square ($2.8^\circ \times 2.8^\circ$) nearest to the station.

3.2 Transport of PAN into the UTLS due to monsoon convection

Figure 2a shows the vertical distribution during the annual cycle of the MIPAS-E PAN climatology (for the period 2002–2011) averaged over the ASM region (10–40° N; 60–120° E). ECHAM5-HAMMOZ-simulated PAN mole fractions are smoothed with the averaging kernel of MIPAS. The monthly distribution clearly shows elevated levels of PAN in the UTLS during the ASM season (June–September). Seasonal variation of ECHAM5-HAMMOZ simulated PAN (obtained from reference experiment) over this region is plotted in Fig. 2b for comparison. It also indicates plumes rising into the UTLS during the ASM season, although PAN mole fractions are less than those obtained from MIPAS-E especially during July and August. These differences may be due to uncertainties in VOC, NO_x emissions, chemistry represented in the model, transport errors and coarse model resolution. Also, MIPAS-E views the atmosphere from above and there are uncertainties in the MIPAS-E retrievals. The cross-section plots of differences in MIPAS-E PAN with model-simulated PAN (see Fig. S4 in the Supplement) indicate that in the UTLS (8–23 km), MIPAS-E PAN is higher than model-simulated PAN by ~ 20 –60 ppt (except above 20 km). It is lower by 20–40 ppt over the eastern part of anticyclone (southern India and southeast Asia) and 20–40 ppt over Indonesia and northern Australia. Near the South Pole, MIPAS-E PAN is higher than in ECHAM5-HAMMOZ by 20–90 ppt. The model could not produce high PAN concentrations near the South Pole between 17 and 23 km. In general, in the ASM region during the monsoon season, MIPAS-E PAN is higher than the model by 30–60 ppt between 8 and 16 km and model biases vary between +40 ppt and -40 ppt between 17 and 23 km. The compar-

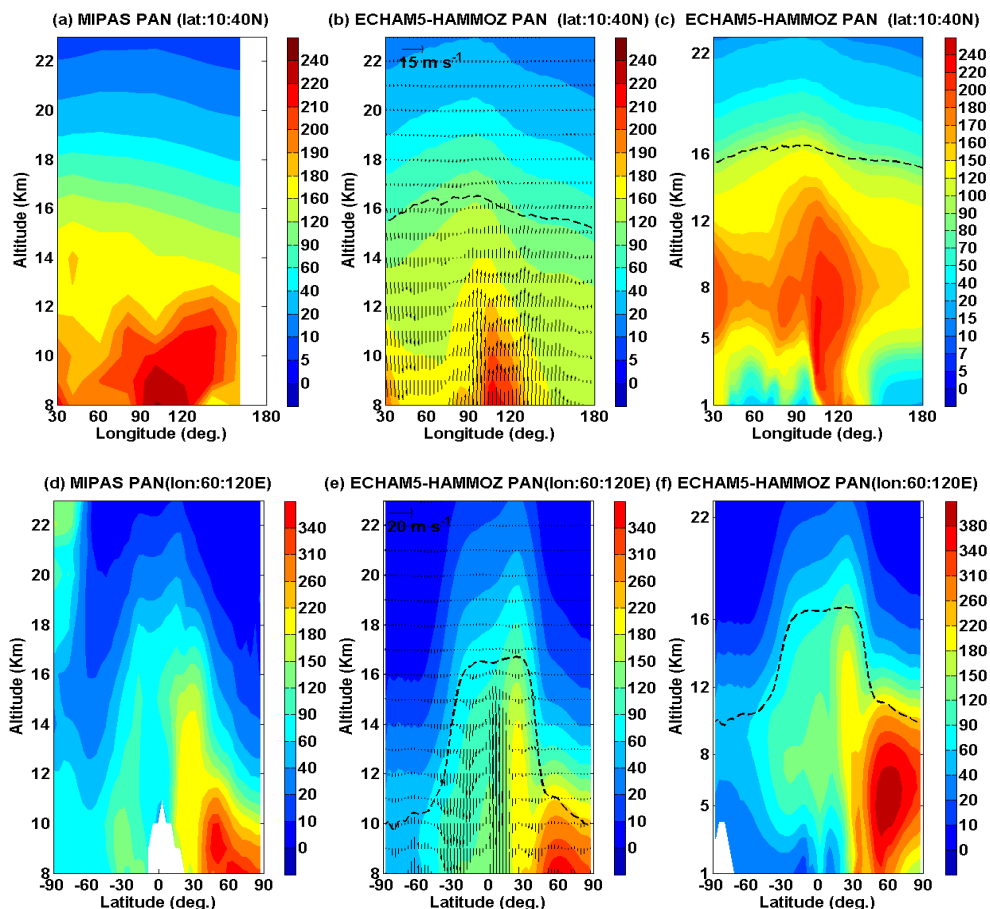


Figure 3. Longitude–altitude cross section of PAN (ppt) averaged for the monsoon season and 10–40° N: (a) MIPAS (climatology for the period 2002–2011) and (b) ECHAM5-HAMMOZ reference simulation between 8 and 23 km. The black arrows indicate wind vectors. The vertical velocity field has been scaled by 300. Panel (c) is the same as figure (b) but from the surface. Latitude–altitude cross section of PAN (ppt) averaged for the monsoon season and 60–120° E for (d) MIPAS climatology and (e) ECHAM5-HAMMOZ reference simulation between 8 and 23 km; (f) same as (e) but from the surface. ECHAM5-HAMMOZ simulation is smoothed with averaging kernels of MIPAS.

ison of PAN measurements from MIPAS-E with the Atmospheric Chemistry Experiment-Fourier Transform Spectrometer (ACE-FTS) indicates MIPAS-E PAN is higher than ACE-FTS in the UTLS by 70 ppt at the altitudes between 9.5 and 17.5 km, which lies within limits of measurement error (Tereszchuk et al., 2013). This indicates that model-simulated PAN concentrations in the UTLS show reasonable agreement with MIPAS-E.

The observed high concentrations during the monsoon season may be due to transport from the lower troposphere due to strong convection and partially due to lightning activity. Thus, in order to study the influence of ASM circulation on the distribution of PAN in the UTLS region, the seasonal mean PAN concentrations (June–September) are analyzed. We present here estimates of the PAN climatology from MIPAS-E for the ASM season. Figure 2c and d exhibit the seasonal mean distribution of PAN as observed by MIPAS at 14 km and 16 km, respectively. PAN distributions obtained from ECHAM5-HAMMOZ reference simulations at

14 and 16 km are plotted in Fig. 2e and f respectively for comparison. Figure 2c–d shows maxima in PAN concentrations (~200–250 ppt) over the Asian monsoon anticyclone region (12–40° N, 20–120° E). The model is able to reproduce the maximum in PAN in the monsoon anticyclone, but simulated PAN concentrations are less than MIPAS observations.

To illustrate vertical transport in the Asian monsoon region, longitude–altitude cross sections averaged over the monsoon anticyclone region 10–40° N and for June–September as obtained from MIPAS PAN observations and ECHAM5-HAMMOZ baseline simulations (8–23 km) are shown in Fig. 3a and b, respectively. Both MIPAS observations and ECHAM5-HAMMOZ simulations show elevated levels of PAN (200–250 ppt) over the foothills of the Himalayas (80–100° E) and pollution sources in Europe and Asia. The vertical winds plotted in Fig. 3b show cross-tropopause transport from the region 80–100° E. Figure 3c reveals that the transport of boundary layer PAN to UTLS

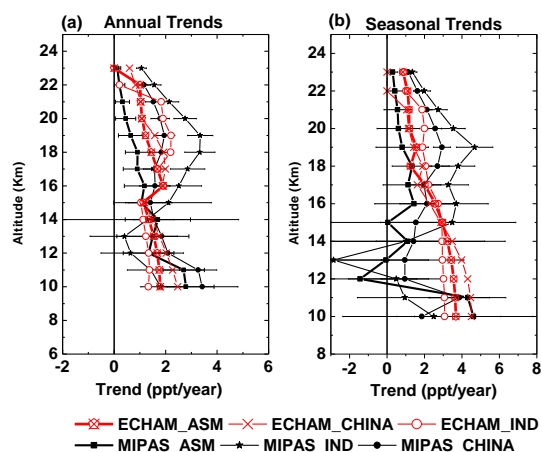


Figure 4. Vertical variation of trends obtained from monthly mean MIPAS-E PAN concentrations averaged for the period 2002–2011 and Ind38Chin73 simulations over the Asian summer monsoon, Chinese and Indian regions (a) annual trends (b) seasonal (June–September) trends.

is mainly from the strong convection regions of the South China Sea ($\sim 100\text{--}120^\circ\text{E}$) and southern flank of the Himalayas ($\sim 80\text{--}90^\circ\text{E}$). In agreement with our results, previous studies also indicate significant vertical transport due to strong monsoon convection from the southern slopes of the Himalayas (Fu et al., 2006; Fadnavis et al., 2013) and the South China Sea (Park et al., 2009). The climatology of the Advanced Very High Resolution Radiometer (AVHRR), Atmospheric Infrared Sounder (AIRS) and Moderate Resolution Imaging Spectroradiometer (MODIS) observations show frequent deep convection over the Bay of Bengal and over the foothills of the Himalayas (Devasthale and Fueglistaler, 2010). From trajectory analysis, Chen et al. (2012) reported that the three dominant regions contributing to transport from the boundary layer to the tropical tropopause are (i) the region between the tropical western Pacific and the South China Sea (38 %), (ii) the Bay of Bengal and southern Asian subcontinent (BOB, 21 %) and (iii) the Tibetan Plateau including the southern slope of the Himalayas (12 %).

The latitude–altitude cross section of MIPAS-E PAN concentrations (averaged over $60\text{--}120^\circ\text{E}$) shows high levels of PAN over the northern subtropics ($20\text{--}40^\circ\text{N}$) (see Fig. 3d). The model-simulated PAN shows a similar distribution (see Fig. 3e). The simulated PAN distribution at the surface reveals that the observed high levels of PAN in the UTLS are from the subtropical boundary layer (see Fig. 3f) and are then transported upwards in deep convection. The PAN is also transported from $40\text{--}60^\circ\text{N}$ reaching up to 16 km. This plume is related to the biomass burning activity during this season over northeast China, Siberia, and Mongolia (figures not shown). The biomass-burning emissions estimated from satellites show intense biomass burning activity over these

regions during monsoon season (Choi et al., 2013). In agreement with our results, ACE-FTS PAN measurements also shows plume concentrations >280 pptv rising from Siberia (Tereszchuk et al., 2013).

The boundary layer lofting of PAN by deep convection may increase NO_x and hence change the ozone concentrations in the UTLS and at remote locations, where it gets transported by the Brewer–Dobson circulation (Randel et al., 2010). Another model simulation study indicates that PAN increases ozone production by removing NO_x from regions of low ozone production efficiency and injecting it into regions with higher ozone production efficiency, resulting in a global increase in ozone production of 2 % (Walker et al., 2010). The strong lightning activity during the monsoon season (Ranalkar and Chaudhari, 2009; Penki and Kamra, 2013) enhances the concentrations of PAN species through production of NO_x (Tie et al., 2001, 2002; Labrador et al., 2005; Zhao et al., 2009; Cooper et al., 2009), which is released into a background atmosphere with some traces of VOCs. MOZART model simulations show that lightning enhances PAN emissions by $\sim 20\text{--}30\%$ and HNO_3 by $\sim 60\text{--}80\%$ in the middle troposphere (Tie et al., 2001). ECHAM5-HAMMOZ simulations show lightning increase in NO_x of $\sim 50\text{--}70\%$, O_3 $\sim 20\text{--}35\%$, HNO_3 $\sim 50\text{--}75\%$ and PAN $\sim 20\text{--}35\%$ over the ASM, respectively (Fadnavis et al., 2014).

4 Trends in PAN in the UTLS of ASM region

Trends in PAN have been computed from MIPAS-E observation in the UTLS (8–23 km), over the ASM region ($10\text{--}40^\circ\text{N}$, $60\text{--}120^\circ\text{E}$), India ($8\text{--}35^\circ\text{N}$, $70\text{--}94^\circ\text{E}$) and China ($20\text{--}45^\circ\text{N}$, $85\text{--}130^\circ\text{E}$). The trends are estimated with the method presented by Von Clarmann et al. (2010). To estimate vertical profiles of annual and seasonal trends, we took into account altitude dependent fit parameters: (1) a possible bias between the PAN values of the 2002–2004 and 2005–2011 measurement periods (details are documented by Von Clarmann et al., 2010), (2) amplitude and phase of the quasi-biennial oscillation (QBO) and (3) amplitudes and phases of periodic variations with periods of 3, 4, 6 and 12 months. The estimated trends are not significant at the altitudes between 8 km and 9 km due to the small number of data points. The trends from model simulations are calculated from the difference between Ind38Chin73 and reference simulations. The estimated annual and seasonal trends are shown in Fig. 4a and b, respectively. Model-simulated and MIPAS-E-observed PAN in the UTLS shows positive trends. The trends obtained from MIPAS-E observations are statistically significant at 2σ (except at few altitudes). The annual trends in MIPAS-E PAN vary between 0.1 ± 0.05 and 2.7 ± 0.8 ppt yr $^{-1}$ over the ASM region, $0.4 \pm 1.3\text{--}3.2 \pm 0.49$ ppt yr $^{-1}$ over India and $1.1 \pm 0.25\text{--}3.4 \pm 1.3$ ppt yr $^{-1}$ over China. Trends over India are insignificant between 12 and 14 km. Figure 4a

shows that in the upper troposphere (10–14 km), trends are higher over China as compared to India. In general, the trend values are higher near the tropopause (~18–19 km). The trends computed from model simulations are of smaller values than the trends obtained from MIPAS-E observations. This may be due to the fact that the simulations do not account for any increase in VOC emissions. However, they show similar regional variations. The model estimated trends over the ASM region vary between 0.1 and 1.9 ppt yr⁻¹, India ~0.2–2.2 ppt yr⁻¹ and China ~0.8–2.4 ppt yr⁻¹. The increases in transportation, industrialization and the number of coal-burning power plants result in the increase of NO_x over southern and eastern Asia. The satellite-observed positive trends of NO_x emissions over these regions (Ghude et al., 2013; Schneider and van der A, 2012) show coherence with estimated trends in MIPAS-E PAN. The estimated trends in MIPAS-E PAN during the monsoon season are larger than annual trends at the altitude above 16 km for all the three regions. At the altitudes below 14 km, seasonal trends are less than annual trends.

During the monsoon season, the estimated trends are positive and statistically significant at 2σ. Over India the seasonal trends in MIPAS-E PAN vary between 0.5 ± 0.8 and 2.7 ± 0.47 ppt yr⁻¹. In the upper troposphere, observed trends are statistically insignificant and they are negative between 12 and 14 km. The trends are higher over China than India varying between 0.95 ± 1.2 and 2.9 ± 0.45 ppt yr⁻¹, indicating that Chinese emissions contribute more to the anticyclone. The statistically insignificant positive and negative trends in the upper troposphere over India may be related to convective transport and removal of NO_x by wet scavenging in the region near the southern part of Himalayas (Fadnavis et al., 2014). Model simulations for enhanced NO_x emissions over India show a nonlinear increase in PAN in the upper troposphere (see the discussions in Sect. 5.3). The variation of trends during the monsoon season computed from ECHAM5-HAMMOZ PAN is similar to the trends obtained from MIPAS-E PAN although the estimated trends are lower. Trends vary in the ranges of ~0.9–3 ppt yr⁻¹ over India, ~1–4.5 ppt yr⁻¹ over China and ~0.8–3.6 ppt yr⁻¹ over ASM.

Trends are larger over China than India in the upper troposphere and vice versa in the lower stratosphere. The 73 % change in emissions over China involves larger total emissions than the 38 % change over India since China emits more than India. Most of the Indian emissions are lofted to higher altitudes than the Chinese emissions by the deep convective system at the southern slopes of the Himalayas. However, a fraction of the Chinese emissions are lofted via this convective transport as well. The role of relatively shallower convective systems in lofting Chinese emissions is greater compared to India (details are given in Sect. 5). Satellite observations show higher tropospheric NO_x concentrations over China compared to India (Schneider and van der A, 2012; Ghude et al., 2013). Because of higher absolute NO_x concentrations over China, the same percent change in emis-

sions will lead to a larger PAN trend in this region compared to India. The amount of PAN-observed in the anticyclone over the ASM region depends on the transport pathways of the air mass. During the monsoon season, the air mass in the anticyclone is from polluted regions of Asia. The polluted air (NO_x and VOCs) from these regions transports high amount of PAN into the UTLS where temperatures are colder; hence, it will retain more of PAN (Nowak et al., 2004).

The positive trends in lightning activity during monsoon season (Penki and Kamra, 2013; Yang and Li, 2014) will increase lightning-induced reactive nitrogen (NO_x) and nitrogen reservoir species (HNO₃, PAN). The lightning-produced PAN is readily carried by convective updrafts to the lower stratosphere, where its lifetime is considerably longer (Labrador et al., 2005). The increase in frequency of deep convective clouds over the tropical land mass (Aumann and Ruzmaikin, 2013) may cause an increase in the frequency of vertical transport. Radar, AVHRR, AIRS and MODIS satellite observations show frequent overshoots deep into the tropical tropopause layer during monsoon season (Devasthale and Fueglistaler, 2010; Hassim et al., 2014). The vertical distribution of the seasonal trend suggests that there is a positive trend in transport of PAN into the lower stratosphere due to deep monsoon convection. Thus, observed increase in UTLS PAN during the monsoon season is related to positive trends in (1) emissions at the surface, (2) frequency of overshooting convection and (3) production from lightning.

In general, the trends estimated from MIPAS-E and ECHAM5-HAMMOZ PAN are larger over China than India at altitudes below 14 km and vice versa above 14 km. This may be related with the amount of pollution outflow in the upper troposphere and lower stratosphere from India and China. The pollution from China released primarily below 14 km, and Chinese emissions dominate Indian emissions. The pollution from India has substantial outflow above 14 km due to convective lifting from the southern slopes of the Himalayas.

5 Impact of enhanced anthropogenic Asian NO_x on PAN, HNO₃ and O₃

The satellite observations and model simulations indicate that boundary layer pollutants are lofted into the UTLS by monsoon convection (Randel et al., 2010; Fadnavis et al., 2013, 2014). In the UTLS, transport occurs through the monsoon anticyclone and across the tropopause (Fadnavis et al., 2013). The transport of boundary layer Asian NO_x into the UTLS due to monsoon convection is evident in model simulations (see Fig. S5 in the Supplement). In order to better understand the impact of enhanced anthropogenic Asian NO_x emissions lofted to UTLS by ASM convection on the distribution of PAN, HNO₃ and ozone, we calculate the percentage change of these constituents for the Ind38, Chin73, Ind38Chin38, Ind38Chin73 and Ind73 simulations with re-

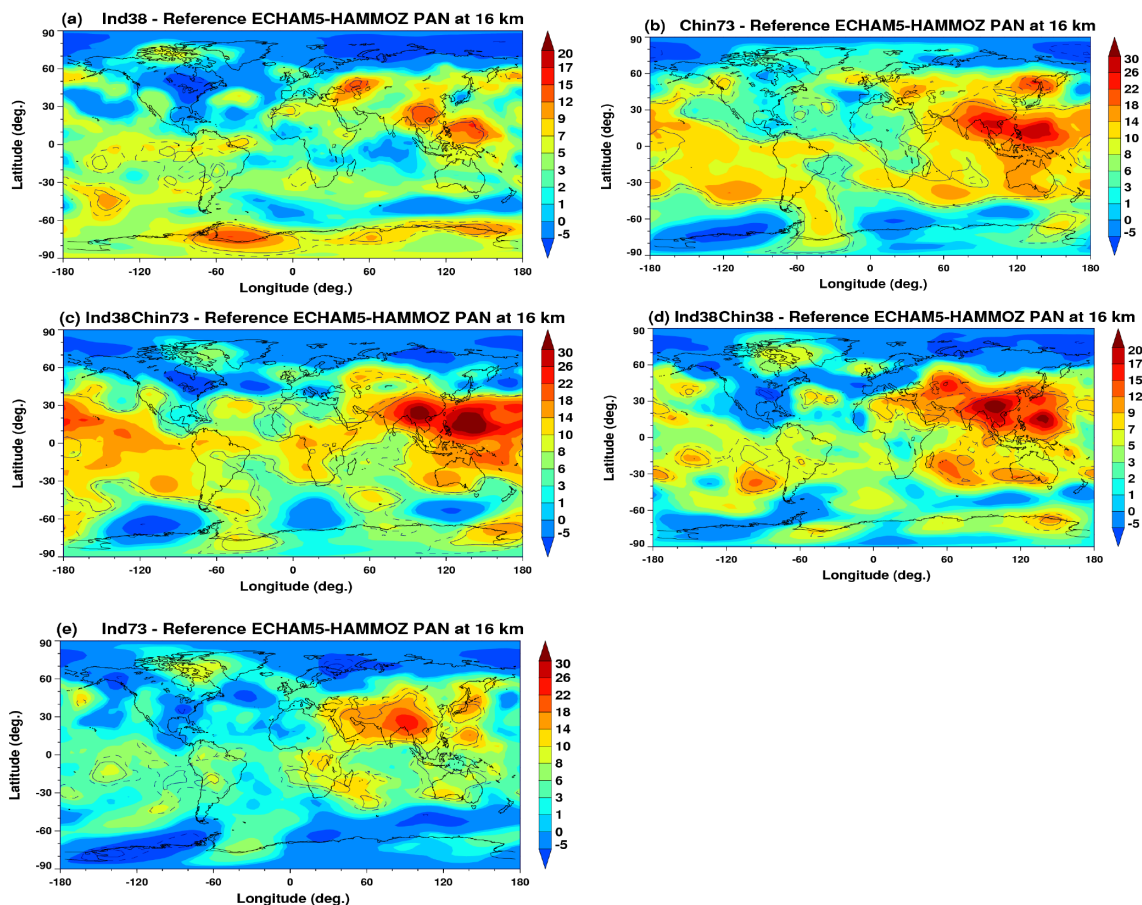


Figure 5. Percentage change in ECHAM5-HAMMOZ PAN at 16 km, as obtained from (a) Ind38, (b) Chin73, (c) Ind38Chin73, (d) Ind38Chin38 and (e) Ind73 simulations. Solid black line indicates the 95 % Student's *t* test confidence interval while the dashed line indicates 90 % confidence interval.

spect to reference simulations. Although we have analyzed horizontal (latitude–longitude) cross sections at different altitudes within the UTLS (8–23 km), here we present plots only at 16 km as a representative of the tropical UTLS layer.

5.1 Impact on PAN

Figure 5a–e show the percentage change in PAN at 16 km for the Ind38, Chin73, Ind38Chin73, Ind38Chin38 and Ind73 simulations. The Ind38 simulation shows an increase in PAN of ~ 10 – 18 % with a 95 % significance level over China and the western Pacific Ocean between Indonesia and Japan. Similar high increases also occur over the northern Caspian Sea and the Weddell Sea near Antarctica. The increase in PAN is ~ 1 – 6 % over most of the other regions in the mid- and low latitudes. PAN decreases in polar regions reflecting a change in the diabatic circulation transport with enhanced descent of low PAN air at high latitudes in the stratosphere.

The Chin73 simulations show an increase in PAN of ~ 18 – 30 % over China and the western Pacific Ocean between Indonesia and Japan and 10 – 18 % over India. An increase in

PAN of ~ 20 % is seen to the north of Japan and ~ 15 % over the Black Sea, southern Pacific Ocean, southern Indian Ocean and Australia. The increase in PAN over other sub-polar regions is ~ 1 – 6 %. During the monsoon season, the westerly winds in the upper troposphere transport NO_y from China eastward over the Pacific Ocean. The increased values in the Southern Hemisphere mid-latitudes similar to the maxima in the Northern Hemisphere mid-latitudes indicate a change in the baroclinic eddy storm tracks. Since the PAN in the extratropics shown in Fig. 5 is in the lowermost stratosphere, it is the change in the Rossby waves penetrating from the tropospheric storm tracks that is producing the anomaly structure. This is not a long-range transport feature but a reflection of a change in the circulation.

The Ind38Chin73 simulations (Fig. 5c) show increases of PAN ~ 14 – 40 % over India, China and the western Pacific and ~ 10 – 20 % over the Pacific Ocean (30°N – 35°S). This gives a combined picture of Ind38 and Chin73 simulations, indicating superposing of trends. The outflow over the Pacific Ocean is more pronounced compared to the Chin73 case, as is to be expected given the Ind38 case shows transport over

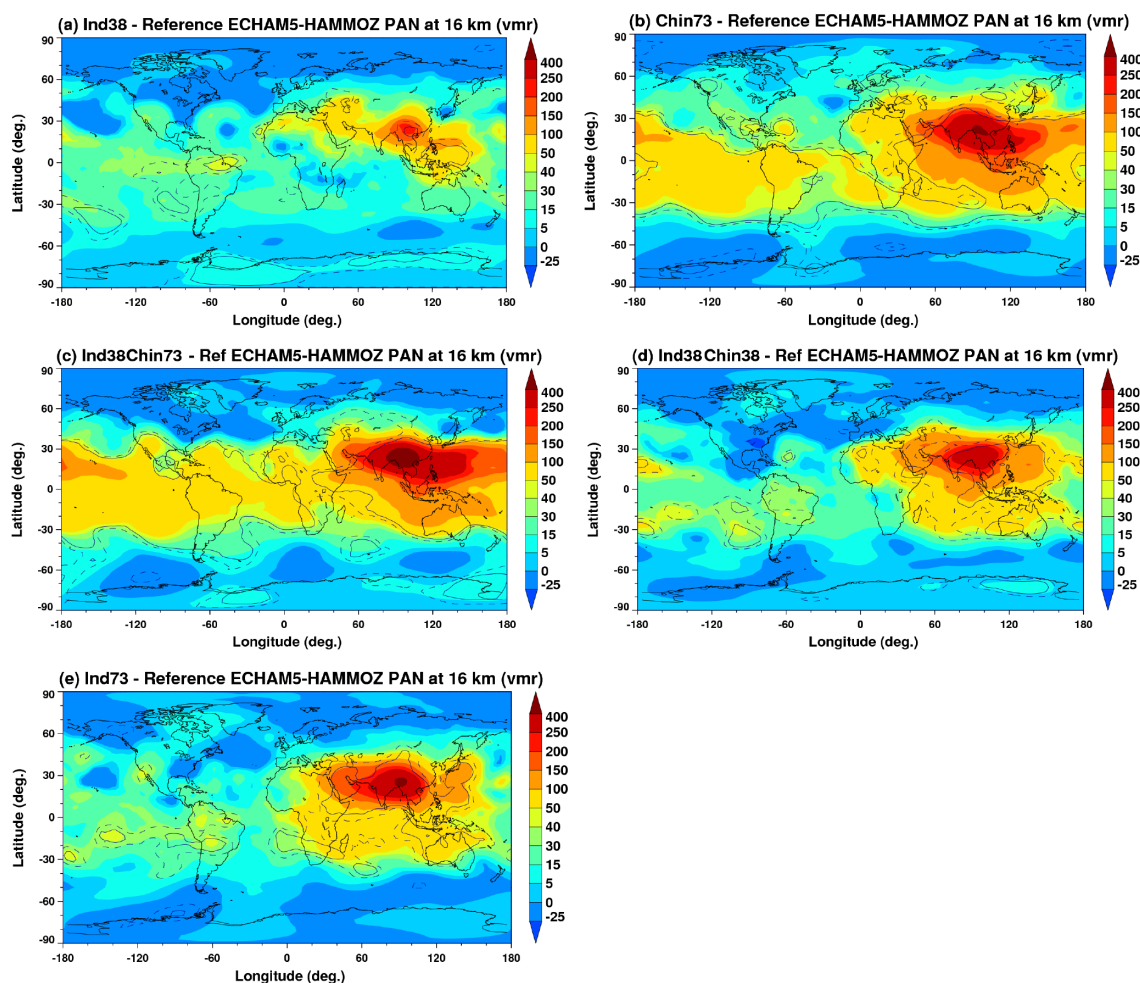


Figure 6. Change in ECHAM5-HAMMOZ PAN at 16 km in ppt, as obtained from (a) Ind38, (b) Chin73, (c) Ind38Chin73, (d) Ind38Chin38 and (e) Ind73 simulations. Solid black line indicates the 95 % Student's t test confidence interval while the dashed line indicates 90 % confidence interval.

the western Pacific. The percentage increase of PAN in the Ind38Chin38 simulations (Fig. 5d) shows a ~ 10 – 25 % increase over India, China and the western Pacific Ocean as in the previous cases. The pattern of PAN increase seen in the Ind38Chin38 case over central Asia and the Black Sea does not persist in the Ind38Chin73 case with non-uniform emissions increases. We attribute this to changes in the dynamics between these simulations that are induced by feedback from ozone and sulfate aerosol produced from SO_2 oxidation on the radiation. The baroclinic eddy storm track changes are not the same for the two emissions scenarios. Closer to the emissions source regions the PAN response is more linear.

Figure 6a–d show changes of PAN in ppt. The figures for volume mixing ratio are given instead of percent since they more clearly indicate the transport pathways. There is a common pathway for PAN into the UTLS in response to increases in NO_x emissions over both India and China in the strong convective uplift over the region of Nepal at the southern

flanks of the Himalayas. An ensemble simulation with emissions increased by 73 % instead of 38 %, Ind73 (Fig. 5e), produced much higher values of PAN in the anticyclone region but did not produce a significant increase in the outflow over the Pacific Ocean. The increase in PAN for Ind38Chin73 simulation is 5 – 20 % yr^{-1} between 10 and 14 km and 2 – 4 % yr^{-1} at the altitudes between 16 and 22 km over India and China. This is in agreement with observed trends in MIPAS-E PAN 0.5 – 2 % between 10 and 14 km and 2 – 4 % yr^{-1} between 16 and 22 km. Comparison of Ind73 and Chin73 simulations shows that PAN outflow over the Pacific Ocean is due to primarily to Chinese emissions with increased values over most tropical longitudes in the case of the latter. Doubling (~ 1.9 times) the NO_x emissions over India increases the PAN amounts by ~ 4 – 12 % over the ASM region and the western Pacific Ocean in the UTLS. The nonlinear response to increases in NO_x emissions over India and China is related to transport pathways. Analysis of the PAN distributions at

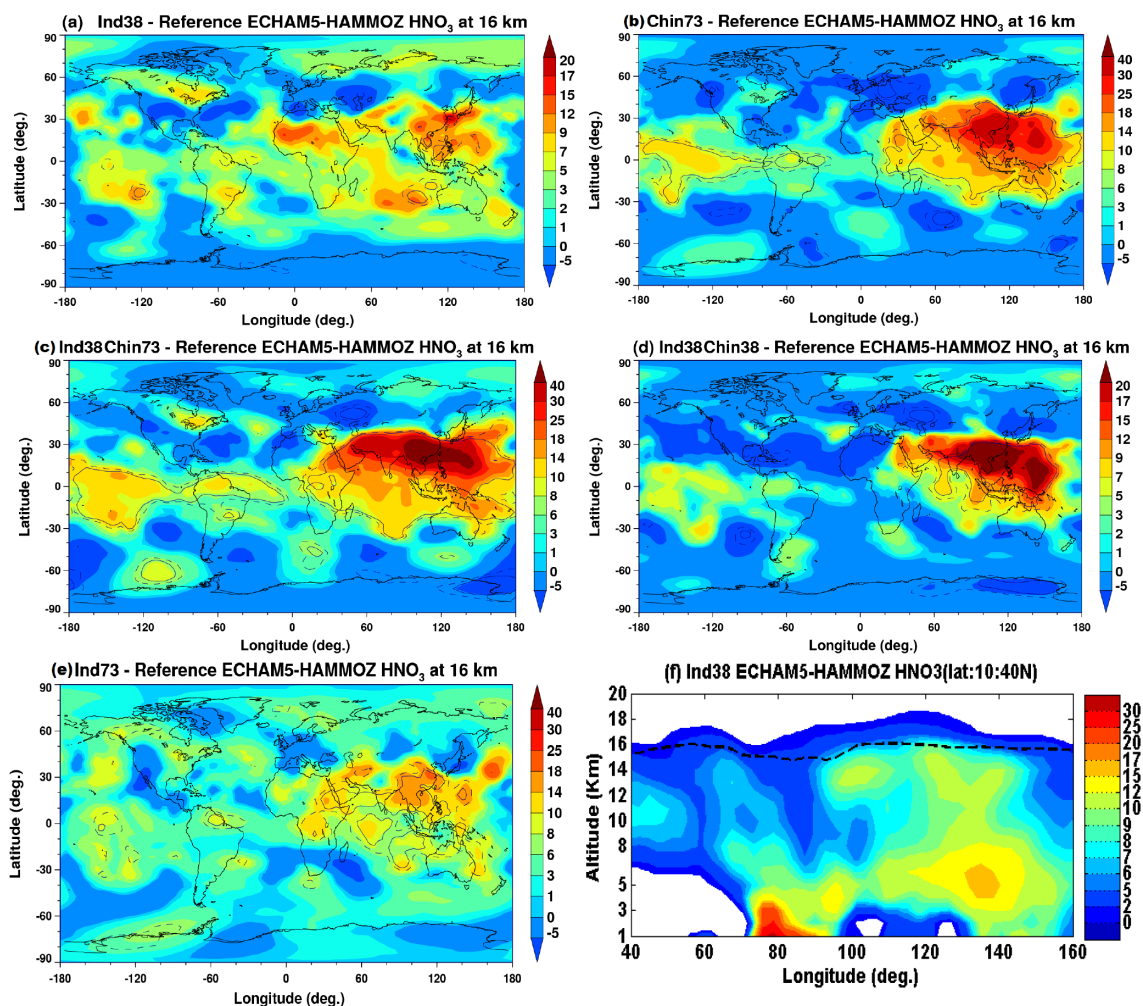


Figure 7. Percentage change in ECHAM5-HAMMOZ HNO_3 at 16 km, as obtained from (a) Ind38, (b) Chin73, (c) Ind38Chin73, (d) Ind38Chin38 and (e) Ind73 simulations. Solid black line indicates the 95 % Student's t test confidence interval while the dashed line indicates 90 % confidence interval (f) Longitude–altitude cross section (averaged over 10–40° N) of percentage change in HNO_3 for the Ind38 simulation.

different altitudes (not shown) indicates that emissions from India enter the UTLS over the region of Nepal, but emissions from China are transported above 8 km over eastern China to the north of Vietnam. In the case of Chinese emissions, PAN is transported over the Pacific Ocean at 8 km and higher altitudes. The Indian emissions are being injected into the ASM anticyclone but a large part of the Chinese emissions enters the UTLS to the east of the anticyclone.

The anticyclone is an effective containment vessel for trace constituents in the UTLS around the tropopause level (Park et al., 2008). Park et al. (2009) found that emissions over India and the Bay of Bengal account for most of the CO in the anticyclone at 100 hPa, and emissions over China make a secondary contribution (see their Figs. 9 and 10). Convective detrainment occurs primarily below 150 hPa, which is the case over China, and only part of it becomes entrained in the anticyclonic circulation with the rest being transported

to the southwest in the Hadley circulation and the northeast over the Pacific Ocean (Jiang et al., 2007; Park et al., 2009).

Another feature apparent in the 16 km distribution of PAN and the other species covered in this section is that the overall change is positive in the tropics and negative in the extratropics. This indicates an intensification of the Brewer–Dobson circulation since there is no chemical mechanism to explain this pattern for all these species. Changes in the synoptic-scale circulation are also evident in the positive and negative tracer anomaly structures in the extratropics. At 16 km, this reflects Rossby wave changes induced by shifting of the baroclinic eddy storm tracks in the troposphere associated with the nonlinear dynamical response to heating perturbations in response to chemical changes.

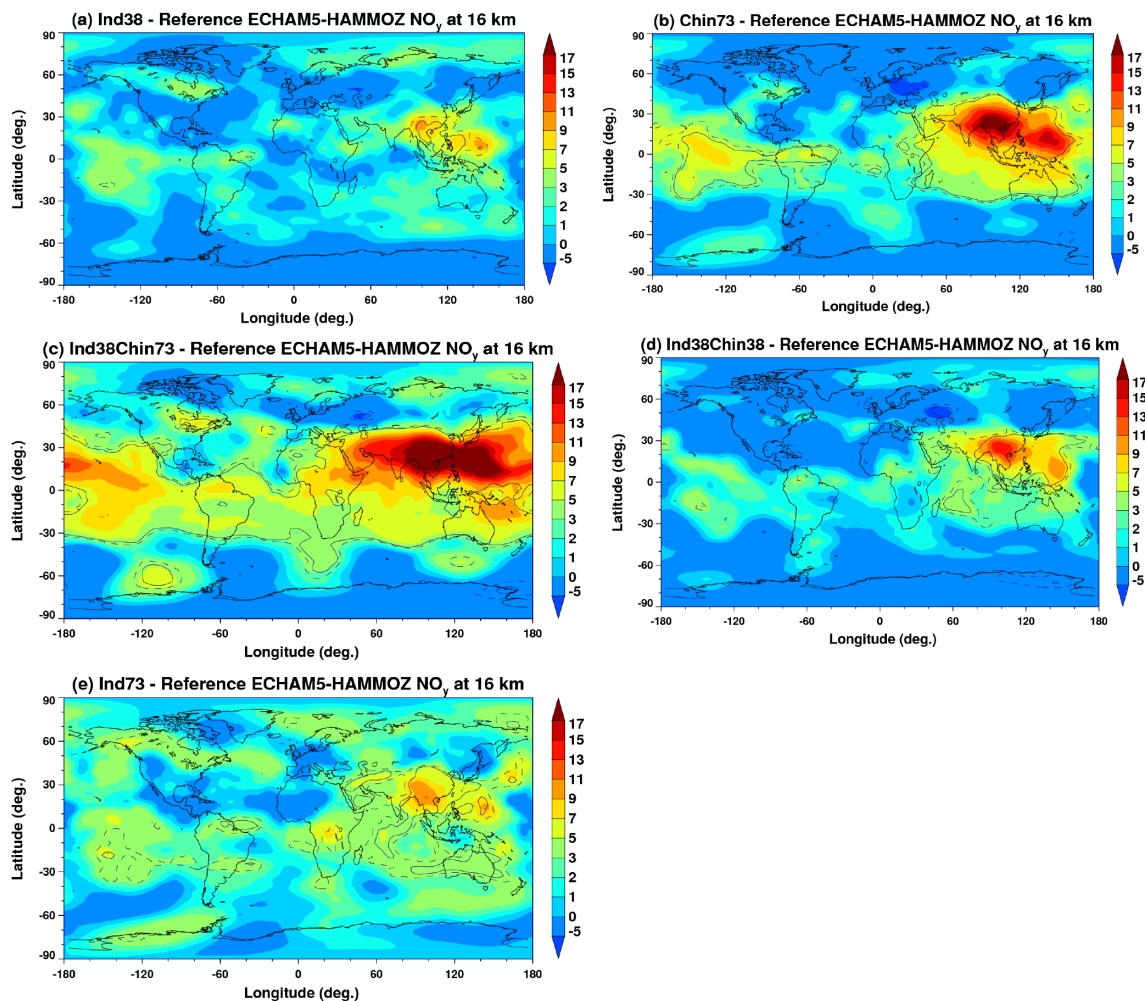


Figure 8. Percentage change in ECHAM5-HAMMOZ NO_y ($\text{NO} + \text{NO}_2 + \text{NO}_3 + 2 \cdot \text{N}_2\text{O}_5 + \text{HNO}_3 + \text{HNO}_4 + \text{PAN} + \text{MPAN} + \text{ONIT} + \text{ONITR} + \text{ISOPNO}_3$) at 16 km, as obtained from (a) Ind38, (b) Chin73, (c) Ind38Chin73, (d) Ind38Chin38, and (e) Ind73 simulations. Solid black line indicates the 95 % Student's t test confidence interval while the dashed line indicates 90 % confidence interval.

5.2 Impact on HNO_3

Changes in the distribution of HNO_3 (%) at 16 km due to enhanced anthropogenic Asian NO_x emissions are shown in Fig. 7a–e. Ind38 simulations show a 1–5 % increase in HNO_3 over most of the regions with a 95 % statistically significant high of 10–14 % over the South China Sea and a high of over 20–25 % over the East China Sea. The Chin73 simulations show an increase in HNO_3 in a region between 30° S and 30° N with few patches over other regions. There is a significant increase in HNO_3 ~14–40 % over the monsoon anticyclone and over 30 % over Southeast Asia, China, the South and East China seas and over the western Pacific Ocean south of Japan. There is an increase (95 % confidence level) in HNO_3 of ~8–14 % over the tropical Pacific Ocean extending to South America. The Ind38Chin73 and Ind38Chin38 simulations show statistically significant increases of HNO_3 in the monsoon anticyclone region. However, when comparing

Indian and Chinese uniform and non-uniform emissions increase cases, it is apparent that a 38 % increase in NO_x emissions over China is not sufficient to drive a significant HNO_3 response over the central and eastern Pacific Ocean. The dynamical response to the NO_x emissions changes is such that HNO_3 is lower in most of the extratropics at 16 km.

5.3 Impact on NO_y

In this section we present impact of enhanced NO_x emissions on NO_y . The NO_y is computed from

$$\text{NO}_y = \text{NO} + \text{NO}_2 + \text{NO}_3 + 2 \cdot \text{N}_2\text{O}_5 + \text{HNO}_3 + \text{HNO}_4 + \text{PAN} + \text{MPAN} + \text{ONIT} + \text{ONITR} + \text{ISOPNO}_3.$$

The impact of enhanced NO_x emissions over India and China (Fig. 8a–e) leads to changes in NO_y (in the UTLS) similar to PAN and HNO_3 (see Figs. 5 and 7). The increase in NO_x emissions over the Indian region leads to an increase of high

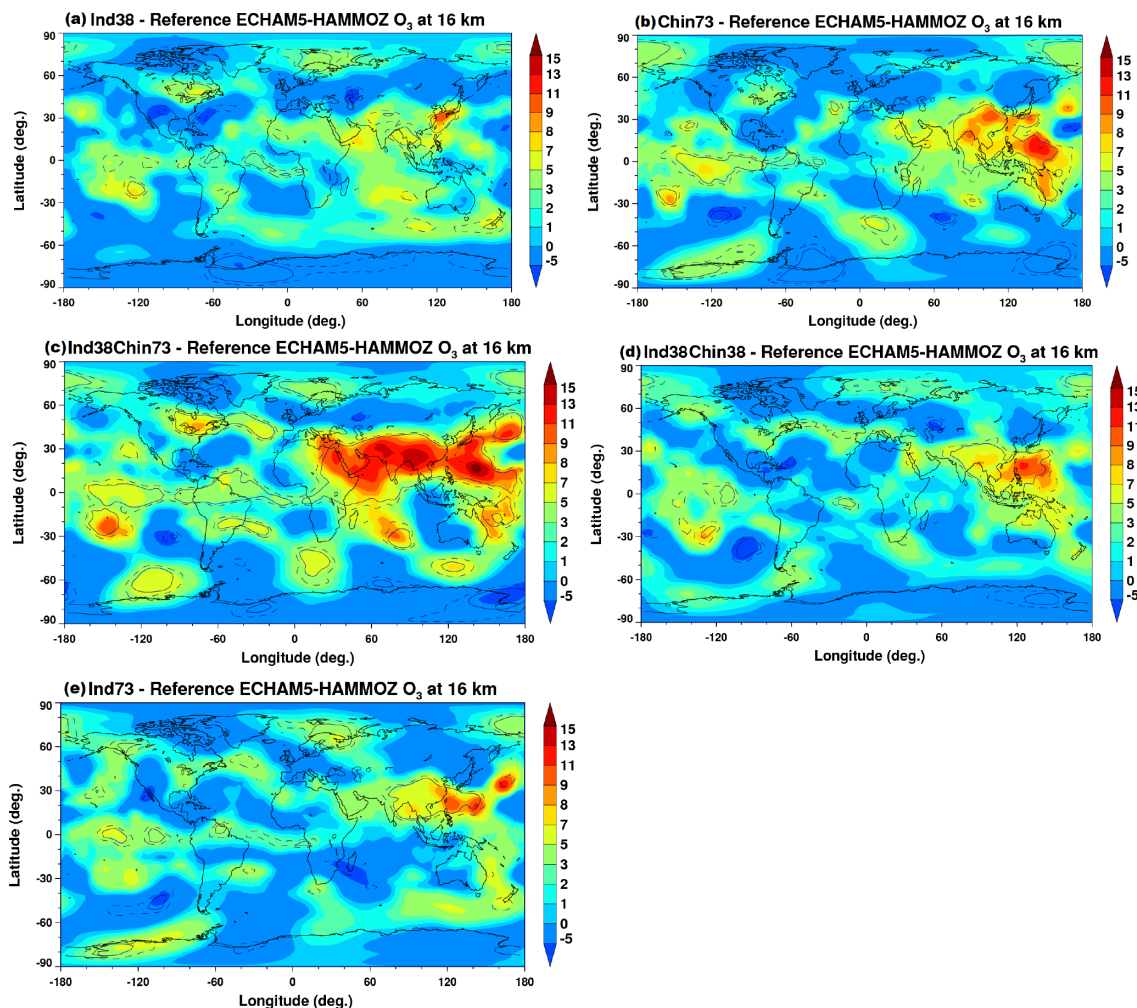


Figure 9. Percentage change in ECHAM5-HAMMOZ ozone at 16 km, as obtained from (a) Ind38, (b) Chin73, (c) Ind38Chin73, (d) Ind38Chin38 and (e) Ind73 simulations. Solid black line indicates the 95 % Student's t test confidence interval while the dashed line indicates 90 % confidence interval.

amounts of NO_y over China (1–11 %) and the western Pacific Ocean (2–11 %), while an increase in NO_x emissions over China increases NO_y over India (2–15 %), Southeast Asia (3–11 %), the South China Sea (7–15 %), the Indian Ocean (3–15 %) and Pacific Ocean (2–15 %).

Figures 5–8 show that increases in NO_x emissions over India increase PAN, HNO_3 and NO_y in the UTLS over Southeast Asia and the South China Sea. Concentrations of these species are lower over the Indian region, especially near southern parts of the Himalaya, from where boundary layer Indian pollutants are transported into the monsoon anticyclone (Fadnavis et al., 2013). However, increase in NO_x emissions over China increases PAN, HNO_3 and NO_y into the monsoon anticyclone. Part of these emissions is taken up by the westerly winds and is transported over the Pacific Ocean. Similar increases in PAN, HNO_3 and NO_y are also observed for the Ind38Chin38 and Ind38Chin73 simula-

tions. The low concentration of HNO_3 , PAN and NO_y over the convection region of the Himalaya may be due to the removal of NO_x by wet scavenging. The ozone distribution at 860 hPa (figure not shown) for the Ind38 simulations shows high anomalies over India, which makes its way over the Pacific Ocean to North America. The longitudinal transect of HNO_3 (see Fig. 7f) indicates that HNO_3 is depleted at around 100°E and this removal process is less effective going farther to the east, i.e., over China and Southeast Asia. It is possible that the extra NO_x over India is being locked up as HNO_3 and removed by wet scavenging. High amount of water vapor present in the atmosphere during the monsoon season may remove NO_x by the reactions $\text{NO}_2 + \text{OH} \rightarrow \text{HNO}_3$ and $\text{N}_2\text{O}_5 + 2\text{H}_2\text{O} \rightarrow 2\text{HNO}_3$ that suggests HNO_3 is more active in the convective zone south of the Himalayas. So the efficiency of NO_x conversion to HNO_3 is larger compared to that over China. A number of previous studies (Holland and

Lamarque, 1997; Shepon et al., 2007) have reported that wet deposition of HNO_3 is the most important pathway of NO_x removal in the free troposphere. The ECHAM5-HAMMOZ analysis of convective heating and vertical ascent in the troposphere over the region of Nepal is more intense than convective systems over China. This indicates that HNO_3 differences are not only due to transport but may reflect differences in wet deposition as well.

5.4 Impact on ozone

Changes in ozone at 16 km due to enhanced Asian anthropogenic NO_x are shown in Fig. 9a–e. An increase in NO_x emissions over India (Ind38) increases ozone (3–7 % or 20–60 ppt) over the Indian Ocean and South China Sea. The Chin73, Ind38Chin38 and Ind38Chin73 simulations show an increase in ozone (3–10 % or 20–100 ppt) over India, the Indian Ocean, Southeast Asia, the South China Sea and the Pacific Ocean, indicating transport by westerly winds. The uniform increase in NO_x over India and China (Ind73 and Chin73) simulations show greater increases in ozone in the monsoon anticyclone in the case of Chinese emissions compared to emissions from India. This is due to removal of NO_x by wet scavenging in the region near the Himalayas. In the stratosphere, the impact of enhanced anthropogenic NO_x emissions is to reduce ozone. ECHAM5-HAMMOZ simulations show a reduction in ozone in the stratosphere (< 70 hPa). The highest ozone loss for the Ind38 simulation is ~ 0.5 –2 % in the stratosphere.

6 Conclusions

Analysis of PAN estimates from MIPAS satellite for the period 2002–2011 and ECHAM5-HAMMOZ global model simulations shows transport of boundary layer PAN into the monsoon anticyclone due to strong convection. The latitude–altitude and longitude–altitude cross-section maps reveal transport mainly occur from the strong convection regions of the South China Sea (~ 100 – 120° E) and the southern flank of the Himalayas (~ 80 – 90° E). These results are in agreement with previous studies (Fu et al., 2006; Park et al., 2009; Chen et al., 2012; Fadnavis et al., 2013), indicating significant vertical transport by deep convection and diabatic-heating-induced upwelling. However, the model simulations reproduce the main features, e.g., a maximum in monsoon anticyclone and vertical transport into the UTLS and the MIPAS-E PAN values are higher than in the model by ~ 30 –60 ppt. The comparison of MIPAS-E PAN measurements with ACE-FTS indicates that MIPAS-E PAN is higher by ~ 70 ppt at the altitudes between 9.5 and 17.5 km (Tereszchuk et al., 2013).

The MIPAS-E PAN observations in the UTLS over India and China show annual trends in PAN varying between 0.4 ± 1.3 and 3.2 ± 0.49 ppt yr^{-1} over India and 1 ± 0.25 and

3.4 ± 1.3 ppt yr^{-1} over China. The seasonal trends are positive, varying between 0.5 ± 0.8 and 2.7 ± 0.47 ppt yr^{-1} over India and 0.95 ± 1.2 and 2.9 ± 0.45 ppt yr^{-1} over China. In general, the estimated trends are statistically significant at 2σ except in the upper troposphere over India, where positive and negative trends are statistically insignificant. These statistically insignificant trends may be related to convective transport from the southern parts of the Himalaya and removal of NO_x by wet scavenging. Model simulations for enhanced NO_x emissions over India also show a nonlinear increase in PAN in the upper troposphere. The estimated seasonal trends are higher than annual trends at altitudes above 14 km over the Indian, Chinese and ASM regions. This may be due to transport by stronger deep convective activity during the monsoon season as observed in radar, AVHRR, AIRS and MODIS (e.g., Devasthale and Fueglistaler, 2010; Hassim et al., 2014). The observed increasing frequency of overshooting convection over the tropical land mass (Aumann and Ruzmaikin, 2013) indicates an increasing trend in transport across the tropical tropopause in agreement with our results. Quantification of changes in UTLS-PAN due to overshooting convection is beyond the scope of this study. The trends estimated from observations and model simulations are higher over China as compared to India at altitudes below 14 km and vice versa above 14 km. This may be related with the amount of pollution outflow in the upper troposphere and lower stratosphere from India and China. The pollution from China is released primarily below 14 km and Chinese emissions dominate Indian emissions. The pollution from India has substantial outflow above 14 km due to convective lifting from southern slopes of the Himalayas.

The trends estimated from sensitivity simulations for Ind38Chin73 are less than the trends in MIPAS-E PAN as simulations do not account for increases in VOCs. However Ind38Chin73 could reproduce variations similar to MIPAS-E observations, higher trend values over China (compared to India) in the upper troposphere and vice versa in the lower stratosphere. The sensitivity simulations for an increase in NO_x emissions over the Indian region lead to an increase of PAN, HNO_3 and ozone over China and the western Pacific Ocean, while an increase in NO_x emissions over China increases PAN over a larger region covering India, Southeast Asia, the South China Sea, Indian Ocean and Pacific Ocean. A comparison of uniform increases in NO_x over India and China (Ind73 and Chin73) shows that the effects on PAN, HNO_3 and O_3 mixing ratios in the anticyclone are more pronounced for Chinese emissions than for Indian emissions. Doubling (~ 1.9 times) the NO_x emissions over India shows a nonlinear increase in PAN, HNO_3 and O_3 over the ASM and the western Pacific UTLS. The non linear response is related to transport pathways. Emissions over India are injected at the eastern end of the monsoon anticyclone by the deep convection over the southern slopes of the Himalayas. A comparison of the India and China simulations shows an increase in NO_x over India, resulting in lower concentrations

of PAN, HNO₃ over the Indian region especially near southern parts of the Himalaya, from where boundary layer Indian pollutants are transported into the monsoon anticyclone. The low concentration of PAN and HNO₃ over this region is due to removal of NO_x by wet scavenging. This may be due to a higher efficiency of NO_x conversion to HNO₃ over India compared to China. However, an increase in NO_x emissions over China increases PAN and HNO₃ in the monsoon anticyclone. A part of these emissions is taken up by the westerly winds and is transported over the Pacific Ocean as far as the Atlantic. There is also westward transport by tropical easterlies which may explain part of the signal over the Atlantic Ocean in the tropics and the Southern Hemisphere. Cross-equatorial transport into the Southern Hemisphere over the south Indian Ocean occurs as well due to mixing by breaking Rossby waves around the equatorial tropopause and via the meridional overturning, or diabatic, circulation. This indicates that Chinese emissions have a greater impact on the concentrations of these species than Indian emissions.

The Supplement related to this article is available online at doi:10.5194/acp-14-12725-2014-supplement.

Acknowledgements. The authors thank the staff of the High Power Computing Centre (HPC) in IITM, Pune, India for providing computer resources. S. Fadnavis acknowledges with gratitude B. N. Goswami, Director of IITM, for his encouragement during the course of this research.

Edited by: B. N. Duncan

References

- Anderson, J. G., Wilmoth, D. M., Smith, J. B., and Sayres, D. S.: UV Dosage Levels in Summer: Increased Risk of Ozone Loss from Convectively Injected Water Vapor, *Science*, 337, 835–839, 2012.
- Aumann, H. H. and Ruzmaikin, A.: Frequency of deep convective clouds in the tropical zone from 10 years of AIRS data, *Atmos. Chem. Phys.*, 13, 10795–10806, doi:10.5194/acp-13-10795-2013, 2013.
- Bhatt, B. C., Koh, T.-Y., Yamamoto, M., and Nakamura, K.: The Diurnal Cycle of Convective Activity over South Asia as Diagnosed from METEOSAT-5 and TRMM Data, *Terr. Atmos. Ocean. Sci.*, 21, 841–854, doi:10.3319/TAO.2010.02.04.01(A), 2010.
- Chen, B., Xu, X. D., Yang, S., and Zhao, T. L.: Climatological perspectives of air transport from atmospheric boundary layer to tropopause layer over Asian monsoon regions during boreal summer inferred from Lagrangian approach, *Atmos. Chem. Phys.*, 12, 5827–5839, doi:10.5194/acp-12-5827-2012, 2012.
- Choi, K.-C., Woo, J.-H., Kim, H. K., Choi, J., Eum, J.-H. and Baek, B. H.: Modeling of Emissions from Open Biomass Burning in Asia Using the BlueSky Framework, *Asian J. Atmos. Environ.*, 7-1, 25–37, doi:10.5572/ajae.2013.7.1.025, 2013.
- Cooper, O. R., Eckhardt, S., Crawford, J. H., Brown, C. C., Cohen, R. C., Bertram, T. H., Wooldridge, P., Perring, A., Brune, W. H., Ren, X., Brunner, D., and Baughcum, S. L.: Summer-time buildup and decay of lightning NO_x and aged thunderstorm outflow above North America, *J. Geophys. Res.*, 114, D01101, doi:10.1029/2008JD010293, 2009.
- Devasthale, A. and Fueglistaler, S.: A climatological perspective of deep convection penetrating the TTL during the Indian summer monsoon from the AVHRR and MODIS instruments, *Atmos. Chem. Phys.*, 10, 4573–4582, doi:10.5194/acp-10-4573-2010, 2010.
- Dodion, J., Fussen, D., Vanhellemont, F., Bingen, C., Matshvili, N., Gilbert, K., Skelton, R., Turnbull, D., McLeod, S. D., Boone, C. D., Walker, K. A., and Bernath P. F.: Aerosols and clouds in the upper troposphere-lower stratosphere region detected by GOMOS and ACE: Intercomparison and analysis of the years 2004 and 2005, *Adv. Space Res.*, 42, 1730–1742, doi:10.1016/j.asr.2007.09.027, 2008.
- Emmons, L. K., Hauglustaine, D. A., Müller, J.-F., Carroll, M. A., Brasseur, G. P., Brunner, D., Staehelin, J., Thouret, V., and Marengo A.: Data composites of tropospheric ozone and its precursors from aircraft measurements, *J. Geophys. Res.*, 105, 20497–20538, 2000.
- Fadnavis, S., Semeniuk, K., Pozzoli, L., Schultz, M. G., Ghude, S. D., Das, S., and Kakatkar, R.: Transport of aerosols into the UTLS and their impact on the Asian monsoon region as seen in a global model simulation, *Atmos. Chem. Phys.*, 13, 8771–8786, doi:10.5194/acp-13-8771-2013, 2013.
- Fadnavis, S., Semeniuk, K., Schultz, M. G., Mahajan, A., Pozzoli, L., Sonbawane, S., and Kiefer, M.: Transport pathways of peroxyacetyl nitrate in the upper troposphere and lower stratosphere from different monsoon systems during the summer monsoon season, *Atmos. Chem. Phys. Discuss.*, 14, 20159–20195, doi:10.5194/acpd-14-20159-2014, 2014.
- Fiore, A. M., Horowitz, L. W., Purves, D. W., Levy II, H., Evans, M. J., Wang, Y., Li, Q., and Yantosca, R. M.: Evaluating the contribution of changes in isoprene emissions to surface ozone trends over the eastern United States, *J. Geophys. Res.*, 110, D12303, doi:10.1029/2004JD005485, 2005.
- Fischer, E. V., Jacob, D. J., Yantosca, R. M., Sulprizio, M. P., Millet, D. B., Mao, J., Paulot, F., Singh, H. B., Roiger, A.-E., Ries, L., Talbot, R. W., Dzepina, K., and Pandey Deolal, S.: Atmospheric peroxyacetyl nitrate (PAN): a global budget and source attribution, *Atmos. Chem. Phys. Discuss.*, 13, 26841–26891, 2013, <http://www.atmos-chem-phys-discuss.net/13/26841/2013/>.
- Fischer, H. and Oelhaf, H.: Remote sensing of vertical profiles of atmospheric trace constituents with MIPAS limb-emission spectrometers, *Appl. Optics*, 35, 2787–2796, 1996.
- Fischer, H., Birk, M., Blom, C., Carli, B., Carlotti, M., von Clarmann, T., Delbouille, L., Dudhia, A., Ehalt, D., Endemann, M., Flaud, J. M., Gessner, R., Kleinert, A., Koopman, R., Langen, J., Lopez-Puertas, M., Mosner, P., Nett, H., Oelhaf, H., Perron, G., Remedios, J., Ridolfi, M., Stiller, G., and Zander, R.: MIPAS: an instrument, *Atmos. Chem. Phys.*, 8, 2151–2188, doi:10.5194/acp-8-2151-2008, 2008.
- Fu, R., Hu, Y., Wright, J. S., Jiang, J. H., Dickinson, R. E., Chen, M., Filipiak, M., Read, W. G., Waters, J. W., and

- Wu, D. L.: Short circuit of water vapour and polluted air to the global stratosphere by convective transport over the Tibetan Plateau, *Proc. Natl. Acad. Sci. USA*, 103, 5664–5669, doi:10.1073/pnas.0601584103, 2006.
- Ganzeveld, L. and Lelieveld, J.: Dry deposition parameterization in a chemistry general circulation model and its influence on the distribution of reactive trace gases, *J. Geophys. Res.*, 100, 20999–21012, doi:10.1029/95JD02266, 1995.
- Gettelman, A., Kinnison, D. E., Dunkerton, T. J., and Brasseur, G. P.: The impact of monsoon circulations on the upper troposphere and lower stratosphere, *J. Geophys. Res.*, 109, D22101, doi:10.1029/2004JD004878, 2004.
- Ghude, S. D., Kulkarni, S. H., Jena, C., Pfister, G. G., Beig, G., Fadnavis, S., and van der A R. J.: Application of satellite observations for identifying regions of dominant sources of nitrogen oxides over the Indian Subcontinent, *J. Geophys. Res.*, 118, 1–15, doi:10.1029/2012JD017811, 2013.
- Glatthor, N., Von Clarmann T., Fischer, H., Funke, B., Grabowski, U., Höpfner, M., Kellmann, S., Kiefer, M., Linden, A., Milz, M., Steck, T., and Stiller, G. P.: Global peroxyacetyl nitrate (PAN) retrieval in the upper troposphere from limb emission spectra of the Michelson Interferometer for Passive Atmospheric Sounding (MIPAS), *Atmos. Chem. Phys.*, 7, 2775–2787, doi:10.5194/acp-7-2775-2007, 2007.
- Hassim, M. E. E., Lane, T. P., and May, P. T.: Ground-based observations of overshooting convection during the Tropical Warm Pool-International Cloud Experiment, *J. Geophys. Res. Atmos.*, 119, 880–905, doi:10.1002/2013JD020673, 2014.
- Hilboll, A., Richter, A., and Burrows, J. P.: Long-term changes of tropospheric NO₂ over megacities derived from multiple satellite instruments, *Atmos. Chem. Phys.*, 13, 4145–4169, doi:10.5194/acp-13-4145-2013, 2013.
- Holland, E. A., and Lamarque J. F.: Modeling bio-atmospheric coupling of the nitrogen cycle through NO_x emissions and NO_y deposition, *Nutr. Cycl. Agroecosyst.*, 48, 7–24, 1997.
- Horowitz, L. W., Walters, S., Mauzerall, D. L., Emmons, L. K., Rasch, P. J., Granier, C., Tie, X., Lamarque, J., Schultz, M. G., Tyndall, G. S., Orlando, J. J., and Brasseur, G. P.: A global simulation of tropospheric ozone and related tracers, Description and evaluation of MOZART, version 2, *J. Geophys. Res.*, 108, 4784, doi:10.1029/2002JD002853, 2003.
- Jiang, J. H., Livesey, N. J., Su, H., Neary, L., McConnell, J. C., and Richards, N. A. D.: Connecting surface emissions, convective uplifting, and long-range transport of carbon monoxide in the upper troposphere: New observations from the Aura Microwave Limb Sounder, *Geophys. Res. Lett.*, 34, L18812, doi:10.1029/2007GL030638, 2007.
- Keim, C., Liu, G. Y., Blom, C. E., Fischer, H., Gulde, T., Höpfner, M., Piesch, C., Ravegnani, F., Roiger, A., Schlager, H., and Sitenkov, N.: Vertical profile of peroxyacetyl nitrate (PAN) from MIPAS-STR measurements over Brazil in February 2005 and its contribution to tropical UT NO_y partitioning, *Atmos. Chem. Phys.*, 8, 4891–4902, doi:10.5194/acp-8-4891-2008, 2008.
- Labrador, L. J., von Kuhlmann, R., and Lawrence, M. G.: The effects of lightning-produced NO_x and its vertical distribution on atmospheric chemistry: sensitivity simulations with MATCH-MPIC, *Atmos. Chem. Phys.*, 5, 1815–1834, doi:10.5194/acp-5-1815-2005, 2005.
- Li, Q., Jiang, J. H., Wu, D. L., Read, W. G., Livesey, N. J., Waters, J. W., Zhang, Y., Wang, B., Filipiak, M. J., Davis, C. P., Turquety, S., Wu, S., Park, R. J., Yantosca, R. M., and Jacob, D. J.: Convective outflow of South Asian pollution: A global CTM simulation compared with EOS MLS observations, *Geophys. Res. Lett.*, 32, L14826, doi:10.1029/2005GL022762, 2005.
- Nesbitt, S. W., Zhang, R., and Orville, R. E.: Seasonal and global NO_x production by lightning estimated from the optical transient detector (OTD), *Tellus B*, 52, 1206–1215, 2000.
- Nowak, J., Parris, D. D., Neuman, J. A., Holloway, J. S., Cooper, O. R., Ryerson, T. B., Nicks, D. K., Flocke, F., Roberts, J. M., Atlas, E., de Gouw, J. A., Donnelly, S., Dunlea, E., Hubler, G., Huey, L. G., Schauffler, S., Tanner, D. J., Warneke, C., and Fehsenfeld, F. C. S.: Gas-phase chemical characteristics of Asian emission plumes observed during ITCT 2K2 over the eastern North Pacific Ocean, *J. Geophys. Res.*, 109, D23S19, doi:10.1029/2003JD004488, 2004.
- Ohara, T., Akimoto, H., Kurokawa, J., Horii, N., Yamaji, K., Yan, X., and Hayasaka, T.: An Asian emission inventory of anthropogenic emission sources for the period 1980–2020, *Atmos. Chem. Phys.*, 7, 4419–4444, doi:10.5194/acp-7-4419-2007, 2007.
- Park, M., Randel, W. J., Kinnison, D. E., Garcia, R. R., and Choi, W.: Seasonal variation of methane, water vapour, and nitrogen oxides near the tropopause: Satellite observations and model simulations, *J. Geophys. Res.*, 109, D03302, doi:10.1029/2003JD003706, 2004.
- Park, M., Randel, W. J., Gettelman, A., Massie, S. T., and Jiang, J. H.: Transport above the Asian summer monsoon anticyclone inferred from Aura Microwave Limb Sounder tracers, *J. Geophys. Res.*, 112, D16309, doi:10.1029/2006JD008294, 2007.
- Park, M., Randel, W. J., Emmons, L. K., Bernath, P. F., Walker, K. A., and Boone, C. D.: Chemical isolation in the Asian monsoon anticyclone observed in Atmospheric Chemistry Experiment (ACE-FTS) data, *Atmos. Chem. Phys.*, 8, 757–764, doi:10.5194/acp-8-757-2008, 2008.
- Park, M., Randel, W. J., Emmons, L. K., and Livesey, N. J.: Transport pathways of carbon monoxide in the Asian summer monsoon diagnosed from Model of Ozone and Related Tracers (MOZART), *J. Geophys. Res.*, 114, D08303, doi:10.1029/2008JD010621, 2009.
- Penki, R. K. and Kamra, A. K.: Lightning distribution with respect to the monsoon trough position during the Indian summer monsoon season, *J. Geophys. Res.*, 118, 4780–4787, doi:10.1002/jgrd.50382, 2013.
- Pozzoli, L., Bey, I., Rast, J. S., Schultz, M. G., Stier, P., and Feichter, J.: Trace gas and aerosol interactions in the fully coupled model of aerosol-chemistry-climate ECHAM5-HAMMOZ: 1. Model description and insights from the spring 2001 TRACE-P experiment, *J. Geophys. Res.*, 113, D07308, doi:10.1029/2007JD009007, 2008a.
- Pozzoli, L., Bey, I., Rast, J. S., Schultz, M. G., Stier, P., and Feichter, J.: Trace gas and aerosol interactions in the fully coupled model of aerosol-chemistry-climate ECHAM5-HAMMOZ: 2. Impact of heterogeneous chemistry on the global aerosol distributions, *J. Geophys. Res.*, 113, D07309, doi:10.1029/2007JD009008, 2008b.
- Pozzoli, L., Janssens-Maenhout, G., Diehl, T., Bey, I., Schultz, M. G., Feichter, J., Vignati, E., and Dentener, F.: Re-analysis of tro-

- ospheric sulfate aerosol and ozone for the period 1980–2005 using the aerosol-chemistry-climate model ECHAM5-HAMMOZ, *Atmos. Chem. Phys.*, 11, 9563–9594, doi:10.5194/acp-11-9563-2011, 2011.
- Ranalkar M. R. and Chaudhari, H. S.: Seasonal variation of lightning activity over the Indian subcontinent, *Meteorol. Atmos. Phys.*, 104, 125–134, 2009.
- Randel, W. J. and Park, M.: Deep convective influence on the Asian summer monsoon anticyclone and associated tracer variability observed with Atmospheric Infrared Sounder (AIRS), *J. Geophys. Res.*, 111, D12314, doi:10.1029/2005JD006490, 2006.
- Randel, W. J. and Jensen, E. J.: Physical processes in the tropical tropopause layer and their roles in a changing climate, *Nature Geosci.*, 6, 169–176, doi:10.1038/ngeo1733, 2013.
- Randel, W. J., Park, M., Emmons, L., Kinnison, D., Bernath, P., Walker, K. A., Boone, C., and Pumphrey, H.: Asian monsoon transport of pollution to the stratosphere, *Science*, 328, 611–613, 2010.
- Ravishankara, A. R.: Water Vapor in the Lower Stratosphere, *Science*, 337, 809–810, doi:10.1126/science.1227004, 2012.
- Ridley, B. A., Madronich, S., Chatfield, R. B., Walega, J. G., Shetter, R. E., Carroll, M. A., and Montzka, D. D.: Measurements and model simulations of the photostationary state during the Mauna Loa Observatory Photochemistry Experiment: Implications for radical concentrations and ozone production and loss rates, *J. Geophys. Res.*, 97, 10375–10388, doi:10.1029/91JD02287, 1992.
- Roeckner, E., Bauml, G., Bonaventura, L., Brokopf, R., Esch, M., Giorgetta, M., Hagemann, S., Kirchner, I., Kornbluh, L., Manzini, E., Rhodin, A., Schlese, U., Schulzweida, U., and Tompkins, A.: The atmospheric general circulation model ECHAM5: Part 1, Tech. Rep. 349, Max Planck Institute for Meteorology, Hamburg, 2003.
- Sander, S. P., Fried, R. R., Barker, J. R., Golden, D. M., Kurylo, M. J., Wine, P. H., J. Abbatt, P. D., 25 Burkholder, J. B., Kolb, C. E., Moortgat, G. K., Huie, R. E., and Orkin, V. L.: Chemical kinetics and photochemical data for use in atmospheric studies, evaluation number 14, JPL Publ. 02-25, Jet Propul. Lab., Calif. Inst. of Technol., Pasadena, available at: http://jpldataeval.jpl.nasa.gov/pdf/JPL_02-25_rev02.pdf, 2003.
- Sander, S. P., Finlayson-Pitts, B. J., Friedl, R. R., Golden, D. M., Huie, R. E., Keller-Rudek, H., 30 Kolb, C. E., Kurylo, M. J., Molina, M. J., Moortgat, G. K., Orkin, V. L., Ravishankara, A. R., and Wine, P. H.: Chemical Kinetics and Photochemical Data for Use in Atmospheric Studies, Evaluation Number 15, JPL Publication 06-2, Jet Propulsion Laboratory, Pasadena, available at: <http://jpldataeval.jpl.nasa.gov> (last access: July 2006), 2006.
- Schneider, P. and van der A. R. J.: A global single-sensor analysis of 2002–2011 tropospheric nitrogen dioxide trends observed from space, *J. Geophys. Res.*, 117, D16309, doi:10.1029/2012JD017571, 2012.
- Shepon, A., Gildor, H., Labrador, L. J., Butler, T., Ganzeveld, L. N., and Lawrence, M. G.: Global reactive nitrogen deposition from lightning NO_x, *J. Geophys. Res.*, 112, D06304, doi:10.1029/2006JD007458, 2007.
- Singh, H. B., Viezee, W., Chen, Y., Thakur, A. N., Kondo, Y. and Talbot, R. W., Gregory, G. L., Sachse, G. W., Blake, D. R., Bradshaw, J. D., Wang, Y., and Jacob, D. J.: Latitudinal distribution of reactive nitrogen in the free troposphere over the Pacific Ocean in late winter/early spring, *J. Geophys. Res.*, 103, 28237–28246, doi:10.1029/98JD01891, 1998.
- Sinha, V., Kumar, V., and Sarkar, C.: Chemical composition of pre-monsoon air in the Indo-Gangetic Plain measured using a new air quality facility and PTR-MS: high surface ozone and strong influence of biomass burning, *Atmos. Chem. Phys.*, 14, 5921–5941, doi:10.5194/acp-14-5921-2014, 2014.
- Stier, P., Feichter, J., Kinne, S., Kloster, S., Vignati, E., Wilson, J., Ganzeveld, L., Tegen, I., Werner, M., Balkanski, Y., Schulz, M., Boucher, O., Minikin, A., and Petzold, A.: The aerosol-climate model ECHAM5-HAM, *Atmos. Chem. Phys.*, 5, 1125–1156, doi:10.5194/acp-5-1125-2005, 2005.
- Tereszczuk, K. A., Moore, D. P., Harrison, J. J., Boone, C. D., Park, M., Remedios, J. J., Randel, W. J., and Bernath, P. F.: Observations of peroxyacetyl nitrate (PAN) in the upper troposphere by the Atmospheric Chemistry Experiment Fourier Transform Spectrometer (ACE-FTS), *Atmos. Chem. Phys.*, 13, 5601–5613, doi:10.5194/acp-13-5601-2013, 2013.
- Tie, X., Zhang, R., Brasseur, G., and Lei, W.: Global NO_x Production by Lightning, *J. Atmos. Chem.*, 43, 61–74, 2002.
- Tie, X. X., Zhang, R., Brasseur, G., Emmons, L., and Lei, W.: Effects of lightning on reactive nitrogen and nitrogen reservoir species in the troposphere, *J. Geophys. Res.-Atmos.*, 106, 3167–3178, doi:10.1029/2000JD900565, 2001.
- Vernier, J. P., Thomason, L. W., and Kar, J.: CALIPSO detection of an Asian tropopause aerosol layer, *Geophys. Res. Lett.*, 38, L07804, doi:10.1029/2010GL046614, 2011.
- von Clarmann, T., Höpfner, M., Kellmann, S., Linden, A., Chauhan, S., Funke, B., Grabowski, U., Glatthor, N., Kiefer, M., Schieferdecker, T., Stiller, G. P., and Versick, S.: Retrieval of temperature, H₂O, O₃, HNO₃, CH₄, N₂O, ClONO₂ and ClO from MIPAS reduced resolution nominal mode limb emission measurements, *Atmos. Meas. Tech.*, 2, 159–175, doi:10.5194/amt-2-2159-2009, 2009.
- von Clarmann, T., Stiller, G., Grabowski, U., Eckert, E., and Orphal, J.: Technical Note: Trend estimation from irregularly sampled, correlated data, *Atmos. Chem. Phys.*, 10, 6737–6747, doi:10.5194/acp-10-6737-2010, 2010.
- Walker, T. W., Martin, R. V., Donkelaar, A. van, Leaitch, W. R., MacDonald, A. M., Anlauf, K. G., Cohen, R. C., Bertram, T. H., Huey, L. G., Avery, M. A., Weinheimer, A. J., Flocke, F. M., Tarasick, D. W., Thompson, A. M., Streets, D. G., and Liu, X.: Trans-Pacific transport of reactive nitrogen and ozone to Canada during spring, *Atmos. Chem. Phys.*, 10, 8353–8372, doi:10.5194/acp-10-8353-2010, 2010.
- Wiegele, A., Glatthor, N., Hopfner, M., Grabowski, U., Kellmann, S., Linden, A., Stiller, G., and von Clarmann, T.: Global distributions of C₂H₆, C₂H₂, HCN, and PAN retrieved from MIPAS reduced spectral resolution measurements, *Atmos. Meas. Tech.*, 5, 723–734, doi:10.5194/amt-5-723-2012, 2012.
- Wu, Z., Wang, X., Turnipseed, A. A., Chen, F., Zhang, L., Guenther, A. B., Karl, T., and Huey, L. G.: 25 Niyogi, D., Xia, B., and Alapaty, K.: Evaluation and improvements of two community models in simulating dry deposition velocities for peroxyacetyl nitrate (PAN) over a coniferous forest, *J. Geophys. Res.*, 117, D04310, doi:10.1029/2011JD016751, 2012.
- Xiong, X., Houweling, S., Wei, J., Maddy, E., Sun, F., and Barnett, C.: Methane plume over South Asia during the monsoon season:

- Satellite observation and model simulation, *Atmos. Chem. Phys.*, 9, 783–794, doi:10.5194/acp-9-783-2009, 2009.
- Yang, X. and Z. Li, Z.: Increases in thunderstorm activity and relationships with air pollution in southeast China, *J. Geophys. Res. Atmos.*, 119, 1835–1844, doi:10.1002/2013JD021224, 2014.
- Yamaji, K., Ohara, T., Uno, I., Tanimoto, H., Kurokawa, J., and Akimoto, H.: Analysis of the seasonal variation of ozone in the boundary layer in East Asia using the Community Multi-scale Air Quality model: what controls surface ozone levels over Japan?, *Atmos. Environ.*, 40, 1856–1868, 2006.
- Zhao, C., Wang, Y., Choi, Y., and Zeng, T.: Summertime impact of convective transport and lightning NO_x production over North America: modeling dependence on meteorological simulations, *Atmos. Chem. Phys.*, 9, 4315–4327, doi:10.5194/acp-9-4315-2009, 2009.